ACCEPTED MANUSCRIPT

Bounds on edge shear layer persistence while approaching the density limit

To cite this article before publication: Rameswar Singh *et al* 2021 *Nucl. Fusion* in press https://doi.org/10.1088/1741-4326/abfadb

Bounds on Edge Shear Layer Persistence while Approaching the Density Limit

Rameswar Singh and P H Diamond

Center for Astrophysics and Space Sciences, University of California San Diego, 9500 Gilman Dr., La Jolla, California 92093, USA

E-mail: rsingh@ucsd.edu

Abstract. This paper details the theory of edge shear layer collapse as the density approaches the Greenwald density limit. It significantly extends earlier work which was restricted in applicability. The zonal shear flow screening length is calculated for banana, plateau and Pfirsch - Schluter regimes. Poloidal field scaling persists in the plateau regime. Neoclassical screening and drift wave - zonal flow dynamics are combined in a theory, which is then reduced to a predator - prey model. Zonal noise, due incoherent mode coupling, is retained. The threshold condition for edge shear layer collapse is computed, and linked to a critical value of the dimensionless parameter $\rho_s/\sqrt{\rho_{sc}L_n}$. The limiting initial edge density for shear layer collapse is derived and shown to scale favorably with plasma current. Results are discussed in light of density limit and Ohmic phenomenology.

1. Introduction

During the past 50 years, considerable progress in understanding the physics of tokamak confinement has occurred. One important concept which emerged during that evolution was that of multiple confinement states, and the transitions between them [1]. Perhaps the clearest examples of this are the L(Low) and H(High) confinement modes, which are linked by the L→H transition [2–8]. Many other confinement modes and transitions have been identified [9–25]. At the same time, interest in identifying and understanding fundamental limits on performance developed. For example, beta limits [26] have received intensive study. And the importance of the density limit [27] has risen, as design for future devices plan on operation in high density regimes [28]. H mode experiments show a density limit, somewhat lower than Greenwald density, above which H-mode confinement cannot be sustained. This H mode density limit (HDL) causes a return to L mode and sets a limit on H mode performance [29–33]. The Greenwald density limit [27, 34], which is a disruptive limit in L mode, is remarkable in many respects, perhaps most notably for its simplicity. It predicts a linear proportionality between the limiting line averaged density n_G and plasma current I_p, i.e., $n_G \sim I_p$. While the density limit frequently is associated with macroscopic phenomena such as multifaceted asymmetric radiation from the edge(MARFE) [35], MHD activity [36] and disruptions, from the beginning, Greenwald himself emphasized the seemingly central role of particle transport in the density limit [34]. In particular, he observed that shallow pellet injection into plasmas with $\overline{n} \sim n_G$ triggered transient particle increased relaxation to n_G by transport rather than by disruption. Thus, the density limit appeared to be fundamentally a 'soft', transport limit, with disruption ensuing as a secondary consequence of the strong edge cooling due to gas fueling.

Recent work has led to a merger, of sorts, between the two lines of research focusing on

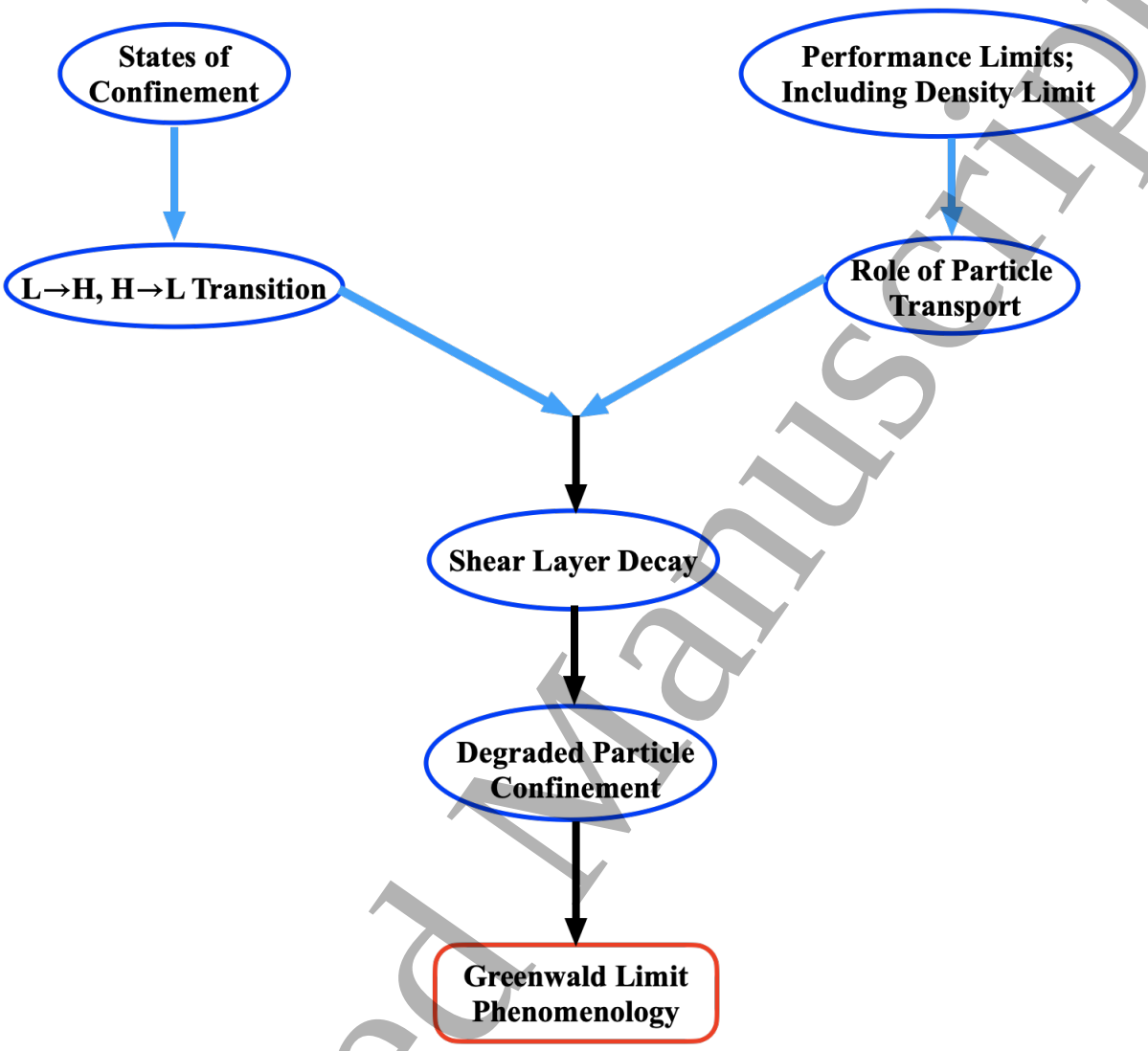

Figure 1. Merging of two lines of research focusing on density limits and confinement transitions.

density limits and confinement transitions, as schematized in figure(1). In particular, two experimental studies have reported findings that link the decay of the ubiquitous edge shear layer (in L mode) and a concomitant increase in turbulent particle flux to the approach $\overline{n}/n_G \rightarrow 1$. This is suggestive of a kind of 'back transition' from a state of turbulence + shear flow to one predominantly of turbulence, as $\overline{n} \rightarrow n_G$. Such a 'back transition' would result in an increase in particle transport and thus a 'stiffening' of the edge density. In particular, Xu *et al* [37] examined the long range correlation (LRC) of edge fluctuations, as $\overline{n}/n_G$ increases. Fluctuation LRC is related to zonal flows, which

exhibit long toroidal correlation on account of their symmetry (i.e., toroidal mode number $n = 0$). Higher LRC means means stronger zonal flows, lower LRC means weaker zonal flows. Xu *et al* [37] found a clear decline in LRC as measured by edge probes as $\overline{n} \rightarrow n_G$, suggestive of decay of the edge shear layer as $\overline{n} \rightarrow n_G$. In a similar vein, Hong *et al* [38] observed an increase in edge particle flux as a decrease in the Reynolds power density coupled from fluctuations to the edge shear layer, while $\overline{n}/n_G$ varied between $0.3 \rightarrow 0.6 \rightarrow 0.8$. In both cases, as $\overline{n}/n_G$ increased, the edge shear layer decayed, and transport increased. Hong *et al* [38] also observed that turbulent particle flux increases and Reynolds power decreases when the adiabaticity parameter $\alpha = k_{\parallel}^2 v_{the}^2/\omega\nu_{ei}$ drops below unity. In a related experiment, Schmid *et al* [39] showed that shear layer production declined, particularly in $\alpha < 1$ plasmas. Detailed analysis contrasted the dominant turbulent fluctuation power transfer processes for $\alpha < 1$ and $\alpha > 1$. Related theoretical work by Hajjar *et al* [40] showed that the decay of the shear flow in $\alpha < 1$ regimes is a consequence of decreased production. To see this, note that for $\alpha > 1$, the wave energy density flux is directly related to the Reynolds stress [41]. Thus causality sets the $\langle k_x k_y \rangle$ correlation - characteristic of the 'eddy tilt' - and thus, the momentum flux. Zonal flow production results. However in the $\alpha < 1$ hydrodynamic regime, the wave energy flux is not simply proportional to the Reynolds stress, so eddy tilting does not arise as a direct consequence of causality. Thus, zonal flow generation is not straightforward in the $\alpha < 1$ regime. Several basic simulations [42–46] confirm this trend of finding waves and zonal flows for $\alpha > 1$, and 2D turbulence for $\alpha < 1$. Finally, detailed analysis by Hajjar *et al* [40] indicates that turbulent viscosity increases for $\alpha < 1$. While the story so far is encouraging, many important issues remain open. The most notable one is the origin of current scaling, so prominent in the Greenwald limit. Another is that the $\alpha < 1$ regime is rather special and likely is not relevant to

even the edges of present day tokamaks. While smaller, cooler devices may support an edge with $\alpha < 1$, larger, hotter devices won't, yet the density limit still is manifested?! More generally, the physics of shear layer decay (especially for $\alpha > 1$) is not yet well understood. The critical edge density for collapse is of great interest, and should be calculated. Finally, we note that the Greenwald limit has not yet been linked to any dimensionless ratios. So, a key question is what dimensionless ratio characterizes the state of the edge shear layer and signals its collapse? Physics, after all, is encoded in dimensionless ratios, so identifying the relevant one is of prime importance.

In this paper, we seek to improve and extend the theory of edge shear layer collapse. The zonal flow screening length $\rho_{sc} \sim \rho_\theta$ is calculated for the banana regime, plateau and Pfirsh-Schluter regimes. Of particular note, we will show that favorable B_θ - scaling of ρ_{sc} persists in the plateau regime, which is relevant in present day edge plasmas [47]. Using the screening results, we "marry" the neoclassical response to the calculations of disparate scale interaction for drift wave - zonal flow turbulence, to derive a coupled system for the evolution of zonal shear flow and drift wave energy. While the major effect here is the familiar "negative viscosity" modulational instability, the model now incorporates neoclassical screening and incoherent mode coupling emission into the zonal modes. We refer to this important effect as 'zonal noise' [48]. The system is then simplified to obtain a $0D$ 'predator - prey' model for turbulence and shear flow, including zonal noise. This model is then analyzed to deduce the condition for shear layer collapse. This condition is determined by turbulence growth, zonal flow damping by viscous diffusion and / or charge exchange friction, and flow - fluctuation coupling. Having obtained the fundamental criterion for flow shear collapse, we then proceed to extract many relevant scalings. The key dimensionless ratio for zonal flow collapse emerges as $\rho_s/\sqrt{\rho_{sc} L_n}$. Note that both ρ_s and ρ_{sc} - a consequence of neoclassical physics

- enter here! We then use particle balance to calculate the initial particle fueling source S_n required to maintain the shear flow. This is readily converted to a limit on the local edge density $n < n_{crit}$, where $n_{crit} \sim B_\theta$ or $\sim B_\theta^2$, depending up on the flow damping. This yields a local edge "density limit", which increases with plasma current! We discuss how turbulent transport responds and increases when shear layer collapses. Our analysis and results are not restricted to the $\alpha < 1$ regime. Finally, we explore the interaction of transport and radiative processes and propose a fueling - heat flux (S_n, Q) 'phase diagram' to describe the states of the edge plasma. Implications for density limit and confinement regimes are discussed in some depth. Some suggestions for experiments are presented.

The remainder of this paper is organized as follows. Section(2) presents the theory of zonal flow screening in banana, plateau and Pfirsch-Schluter regimes. In Section(3), we discuss the dynamics of the drift - wave zonal flow system with neoclassical polarization. The poloidal field dependence of zonal intensity is discussed at length in Section(4). The physics, critical scalings and consequences of the theory are presented in Section(5). The principal results may be found there. Section(6) gives an extended discussion and the conclusions.

2. Zonal flow screening in banana, plateau and Pfirsch-Schluter regimes

In this section, we discuss zonal flow screening. Of course, the zonal flow screening scale is an essential ingredient for determining the edge shear layer structure and strength. We revisit the zonal flow screening calculations of Rosenbluth and Hinton in the banana regime and extend these to Plateau and Pfirsch-Schluter regimes. Note that the original Rosenbluth-Hinton [49] and Hinton-Rosenbluth [50] calculations of zonal flow screening were strictly limited to the banana regime. However, most edge

plasmas fall in the Plateau or Pfirsch-Schluter regimes. The gyro-phase independent ion distribution function f follows

$$\frac{\partial f_k}{\partial t} + \left(v_\parallel \nabla_\parallel + i\omega_d\right) f_k = -\frac{e}{T} F_0 \left(v_\parallel \nabla_\parallel + i\omega_d\right) \phi + C_{ii}(f_k) + S_{ik} \tag{1}$$

where where F_0 is a local Maxwellian, C_{ii} is the linearized ion-ion collision operator, and the magnetic drift frequency is $\omega_d = \vec{k}_\perp \cdot \vec{v}_d$. Here we assume all perturbed quantities take an eikonal form $\phi(\vec{r}, t) = \sum_{\vec{k}} \phi_k(t) e^{i\mathcal{S}}$ with the eikonal $\mathcal{S} = \mathcal{S}(\psi)$ and the radial wave vector $\vec{k}_\perp = \vec{\nabla}\mathcal{S}$. The magnetic drift $\vec{v}_d = \left(\vec{b}/\Omega\right) \times \left(\mu \vec{\nabla} B + v_\parallel^2 \vec{b} \cdot \vec{\nabla}\vec{b}\right)$ has the radial component $\vec{v}_d \cdot \vec{\nabla}\psi = v_\parallel \vec{b} \cdot \vec{\nabla}\left(I v_\parallel/\Omega\right)$. Then, following Hinton and Rosenbluth [50], a convenient form of ω_d can be written as $\omega_d = v_\parallel \nabla_\parallel Q$ where $Q = I\mathcal{S}' v_\parallel/\Omega$. The independent velocity variables used in the preceding equation are $E = v^2/2$ and the magnetic moment $\mu = v_\perp^2/2B$. The source term S_{ik} is nothing but the $E \times B$ convective nonlinearity in the gyrokinetic equation

$$S_{ik} = \frac{c}{B} \sum_{k'} \left(\hat{b} \times \vec{k}' \cdot \vec{k}''\right) J_0(k'_\perp \rho) \phi_{k'} f_{k''} \tag{2}$$

where $\vec{k}'' = \vec{k} - \vec{k}'$, J_0 is a Bessel function and $\rho = v_\perp/\Omega$ is the Larmor radius. To solve equation(1) we decompose the total distribution function into an adiabatic and a non-adiabatic part.

$$f_k = -\frac{e\phi_k}{T_i} F_0 + H_k e^{-iQ} \tag{3}$$

Using the fact that the zonal flow potential is independent of the position along a field line, the non adiabatic distribution function H_k satisfies the following equation:

$$\frac{\partial H_k}{\partial t} + v_\parallel \nabla_\parallel H_k = e^{iQ} \frac{e}{T} F_0 \frac{\partial \phi}{\partial t} + e^{-iQ} C_{ii}(H_k e^{-iQ}) \tag{4}$$

Now in the limit of long wavelength zonal flows $Q << 1$, one can expand H_k as

$$H_k = H_{k0} + H_{k1} + H_{k2} + ... \tag{5}$$

The leading order equation can be written as

$$\frac{\partial H_{k0}}{\partial t} + v_\parallel \nabla_\parallel H_{k0} = \frac{e}{T} F_0 \frac{\partial \phi}{\partial t} + C_{ii}(H_{k0}) \tag{6}$$

This yields the leading order solution:

$$H_{k0} = \frac{e}{T} F_0 \phi_k, \tag{7}$$

since $v_\parallel \nabla_\parallel H_{k0} = C_{ii}(H_{k0}) = 0$. The first order equation is

$$\frac{\partial H_{k1}}{\partial t} + v_\parallel \nabla_\parallel H_{k1} = iQ \frac{e}{T} F_0 \frac{\partial \phi}{\partial t} + C_{ii}(H_{k1}) \tag{8}$$

since $C_{ii}(H_{k0}Q) = 0$ due to momentum conservation in like-like collisions. The second order kinetic equation can be written as

$$\frac{\partial H_{k2}}{\partial t} + v_\parallel \nabla_\parallel H_{k2} = -\frac{Q^2}{2} \frac{e}{T} F_0 \frac{\partial \phi}{\partial t} + C_{ii}(H_{k2}) + iQC_{ii}(H_{k1}) + C_{ii}(iQH_{k1}) \tag{9}$$

The distribution function to order Q^2, can be written as

$$f_k \approx \left(-iQ \frac{e}{T} F_0 \phi_k + H_{k1}\right)(1 - iQ) + \frac{Q^2}{2} \frac{e}{T} F_0 \phi_k + H_{k2} \tag{10}$$

Polarization density: The polarization density is obtained below. The time rate of change of flux surface averaged polarization density $\langle n_{kpol} \rangle = \left\langle \int d^3v f_k \right\rangle$ is

$$\frac{\partial \langle n_{kpol} \rangle}{\partial t} = \left\langle \int d^3v \left[\left(-iQ \frac{e}{T} F_0 \frac{\partial \phi_k}{\partial t} + \frac{\partial H_{k1}}{\partial t} \right)(1 - iQ) + \frac{Q^2}{2} \frac{e}{T} F_0 \frac{\partial \phi_k}{\partial t} + \frac{\partial H_{k2}}{\partial t} \right] \right\rangle \tag{11}$$

Inserting the expressions for $\frac{\partial H_{k1}}{\partial t}$ and $\frac{\partial H_{k2}}{\partial t}$ from equations (8) and (9) in the preceding equation, and utilizing the properties of the linear ion-ion collision operator C_{ii} , one arrives at

$$\frac{\partial \langle n_{kpol} \rangle}{\partial t} = \left\langle \int d^3v \left(-iQ \frac{e}{T} F_0 \frac{\partial \phi_k}{\partial t} + \frac{\partial H_{k1}}{\partial t} \right)(-iQ) \right\rangle \tag{12}$$

. This yields the following expression for the flux surface averaged neoclassical polarization density to $O(Q^2)$

$$\langle n_{kpol} \rangle = -\left\langle \int d^3v \left(iQH_{k1} + \frac{e}{T} F_0 \phi_k Q^2 \right) \right\rangle \tag{13}$$

Now we only need to solve the equation(8) for H_{k1}. Note that this is the most general expression for the flux surface averaged polarization density $\langle n_{kpol} \rangle$ in the long wave length limit. It is valid for all collisionality regimes. To calculate the polarization density in different collisionality regimes H_{k1}, needs to be evaluated accordingly. Then the polarization screening response in frequency ($p = i\omega$) and wave number (k) space follow from

$$\varepsilon^{pol}_{k,nc}(p) \left\langle k_\perp^2 \right\rangle \phi_k(p) = -4\pi e \langle n_{kpol} \rangle \tag{14}$$

2.1. Plateau regime: $\omega_b << \nu_{ii} << \omega_T$

For ease of distinction between trapped and passing particles it is useful to introduce the pitch angle variable $\lambda = \frac{v_\perp^2 B_0}{v^2 B}$ where B_0 is on-axis value of magnetic field and $h \equiv B_0/B = R/R_0 = 1 + \epsilon cos\theta$. Then the velocity element can be written as $d^3v = 4\pi B E dE d\lambda / m^2 B_0 |v_\parallel|$. Using $Q = IS' v_\parallel / \Omega$, the polarization density can be written as:

$$\langle n_{kpol} \rangle = n_0 \frac{e\phi_k}{T} k_\perp^2 \rho_i^2 \frac{B_0^2}{B_\theta^2} \frac{3}{2} \int d\lambda \left[\left\langle \frac{\Omega_0 T_i}{i\sigma IS' v e \phi_k F_0} \int \frac{d\theta}{2\pi} h H_{k1} \right\rangle_E - \int \frac{d\theta}{2\pi} h^2 \zeta \right] \tag{15}$$

where $\zeta = |v_\parallel|/v$ is the dimensionless parallel speed with $\sigma = v_\parallel/|v_\parallel|$ and $h = B_0/B = 1 + \epsilon cos\theta$ for a large aspect ratio circular tokamak, $\epsilon = r/R_0$. The energy average is defined as

$$\langle A \rangle_E = \frac{\int_0^\infty dE E^{3/2} e^{-E/T} A}{\int_0^\infty dE E^{3/2} e^{-E/T}} \tag{16}$$

Using the expression for polarization density from equation(15), the above equation yields

$$\varepsilon^{pol}_{k,nc}(p) = \frac{\omega^2_{pi}}{\omega^2_{ci}}\frac{q^2}{\varepsilon^2}\frac{3}{2}\int d\lambda \left[\int \frac{d\theta}{2\pi} h^2 \zeta - \langle G_k(p)\rangle_E\right] \tag{17}$$

where

$$G_k(p) = \frac{\Omega_0 T_i}{i\sigma I S' v e \phi_k F_0}\int \frac{d\theta}{2\pi} h H_{k1}(p) \tag{18}$$

and $\epsilon = r/R$ is the inverse aspect ratio, $\omega_{pi} = \sqrt{4\pi e^2 n_0/m_i}$ is the ion plasma frequency, $\omega_{ci} = eB_0/m_i$ is the ion gyro frequency at the magnetic axis, and $\rho_i = v_i/\omega_{ci}$ is the ion gyro radius. This form of the expression for $\varepsilon^{pol}_{k,nc}(p)$ is convenient for determining of the separate contributions from trapped particles and passing particles. To solve for H_{k1}, a subsidiary expansion in the smallness parameter $\omega/\omega_T = \epsilon \ll 1$ can be used in equation(8).

$$H_{k1} = H^{(0)}_{k1} + H^{(1)}_{k1} + ... \tag{19}$$

Ordering $\nu/\omega_T = \epsilon \ll 1$, the leading order ($\mathcal{O}(\epsilon^0)$) equation becomes

$$v_\parallel \nabla_\parallel H^{(0)}_{k1} = 0 \tag{20}$$

This implies that H^0_{k1} is independent of poloidal angle θ. The equation at order ($\mathcal{O}(\epsilon^1)$) becomes

$$\frac{\partial H^{(0)}_{k1}}{\partial t} + v_\parallel \nabla_\parallel H^{(1)}_{k1} = iQ\frac{e}{T}F_0\frac{\partial \phi}{\partial t} + C_{ii}(H^{(0)}_{k1}) \tag{21}$$

Now a transit average of the above equation(21) annihilates the second term on the left hand side. Then taking the Laplace transform of the transit averaged equation yields

$$H^{(0)}_{k1}(p) = i\overline{Q}\frac{e}{T}F_0\phi_k(p) + \frac{1}{p}\overline{C_{ii}(H^{(0)}_{k1}(p))} \tag{22}$$

Here the distribution $H_{k1}^{(0)}(p)$ is Laplace transform of $H_{k1}^{(0)}(t)$ and is independent of θ. The transit average is defined as $\bar{A} = \int \frac{d\theta A}{v_\parallel \vec{b}.\vec{\nabla}\theta} / \int \frac{d\theta}{v_\parallel \vec{b}.\vec{\nabla}\theta}$. For trapped particles, this average is over a full bounce; while for passing particles, it is over one complete poloidal circuit. Now since $\nu >> \omega_b$ in Plateau regime, trapping is not effective and hence the trapped population effects can be ignored. This argument leads to

$$\varepsilon_{k,nc}^{pol}(p) = \frac{\omega_{pi}^2}{\omega_{ci}^2}\frac{q^2}{\varepsilon^2}\left[\mathcal{L} - \mathcal{P}(p)\right] \tag{23}$$

where

$$\mathcal{L} = \frac{3}{2}\int_0^{1-\epsilon} d\lambda \oint \frac{d\theta}{2\pi} h^2 \zeta = 1 - \frac{4}{3\pi}(2\epsilon)^{3/2} \tag{24}$$

and

$$\mathcal{P}(p) = \frac{3}{2}\int_0^{1-\epsilon} d\lambda \left\langle G_k(p)\right\rangle_E \tag{25}$$

Note that in banana regime

$$\mathcal{L} = \frac{3}{2}\left[\int_0^{1-\epsilon} d\lambda \oint \frac{d\theta}{2\pi} h^2\zeta + \int_{1-\epsilon}^{1+\epsilon} d\lambda \int_{-\theta_b}^{+\theta_b} \frac{d\theta}{2\pi} h^2\zeta\right] = 1 \tag{26}$$

Now we approximate the ion-ion collision operator by the Lorentz operator,

$$C_{ii}(H_{k1}^{(0)}) = 2\left(\frac{T_i}{m_i E}\right)^{3/2} \nu_{ii}\frac{B_0}{B}\xi\frac{\partial}{\partial\lambda}\lambda\xi\frac{\partial H_{k1}^{(0)}}{\partial\lambda} \tag{27}$$

where the ion-ion collision frequency is $\nu_{ii} = \frac{4\pi e^4 n ln\Lambda}{m_i^{1/2}(2T_i)^{3/2}}$. Hereafter, following the collisional calculation of of Xiao *et al [51],* one arrives at the following (approximate) expression for $\mathcal{P}$

$$\mathcal{P}(p) = \frac{1-\Theta}{1+\Gamma_0/p\tau_{ii}} \tag{28}$$

where $\Theta = 1.6\epsilon^{3/2}$ and $\Gamma_0 = \frac{4(1+1.461\sqrt{\epsilon})}{3\sqrt{\pi}}$ and τ_{ii} is ion-ion collision time. The time evolution of zonal flow potential is given by

$$\begin{aligned}\phi_k(t) &= \phi_k(0)\frac{1}{2\pi i}\int \frac{dp}{p} e^{pt} \frac{\varepsilon^{pol}_{k,cl}}{\varepsilon^{pol}_{k,cl} + \varepsilon^{pol}_{k,nc}(p)} \\ &= \phi_k(0)\frac{\epsilon^2/q^2}{\epsilon^2/q^2 + \mathcal{L}}\left[1 + \frac{1-\Theta}{\epsilon^2/q^2 + \mathcal{L} - 1 + \Theta} e^{-\gamma t}\right] \end{aligned} \tag{29}$$

where the zonal flow damping rate is given by

$$\gamma = \frac{(\epsilon^2/q^2 + \mathcal{L})\,\Gamma_0}{\tau_{ii}\,(\epsilon^2/q^2 + \mathcal{L} - 1 + \Theta)} \tag{30}$$

Therefore, for times much longer than ion-ion collision time,

$$\frac{\phi_k(\infty)}{\phi_k(0)} = \frac{\epsilon^2/q^2}{\epsilon^2/q^2 + \mathcal{L}} \approxeq \frac{\epsilon^2/q^2}{\mathcal{L}} = \frac{1}{\mathcal{L}}\left(\frac{B_\theta}{B_T}\right)^2 \tag{31}$$

Note that for the banana regime, $\mathcal{L} = 1$ and hence

$$\frac{\phi_k(\infty)}{\phi_k(0)} = \frac{\epsilon^2/q^2}{\epsilon^2/q^2 + 1} = \left(\frac{B_\theta}{B_T}\right)^2 \tag{32}$$

This shows that the favorable magnetic field scaling of the residual zonal flow survives in the plateau regime. As a result, the screening length in the banana-plateau regime is $\rho_{sc} = \sqrt{\rho_s^2 + \mathcal{L}\rho_\theta^2} \approx \mathcal{L}^{1/2}\rho_\theta$, where $\mathcal{L} = 1$ for banana regime and $\mathcal{L} < 1$ for plateau regime. This implies the screening length in the plateau regime is smaller than that in the banana regime.

2.2. Pfirsch-Schluter regime $\omega << \omega_T << \nu_{ii}$

In this regime, the collisions are too frequent for particles to complete a single orbit. Hence the transit average of equation(8) is not possible. Making a Chapman-Enskog expansion in the small parameter $\omega/\nu_{ii} \ll 1$

$$H_{k1} = H^0_{k1} + H^1_{k1} + H^2_{k1} + ... \tag{33}$$

in equation(8) yields

$\underline{\epsilon^0}$:

$$C_{ii}(H^0_{k1}) = 0 \tag{34}$$

$\underline{\epsilon^1}$:

$$v_\parallel \nabla_\parallel H^0_{k1} = C_{ii}(H^1_{k1}) \tag{35}$$

$\underline{\epsilon^2}$:

$$\frac{\partial H^0_{k1}}{\partial t} + v_\parallel \nabla_\parallel H^1_{k1} = iQ\frac{e}{T}F_0\frac{\partial \phi_k}{\partial t} + C_{ii}(H^2_{k1}) \tag{36}$$

Again, for the zonal mode one gets:

$$H^0_{k1} = iQ\frac{e}{T}F_0\phi_k + \int dt C_{ii}(H^2_{k1}) \tag{37}$$

which yields

$$\langle n_{kpol} \rangle \;=\; -\left\langle \int d^3v \int dt\, iQC_{ii}(H^2_{k1}) \right\rangle = 0 \tag{38}$$

This immediately gives $\varepsilon^{pol}_{k,nc} = 0$ and hence

$$\left(\frac{\phi_k(\infty)}{\phi_k(0)}\right)_{Pfirsch-Schluter} = 1 \tag{39}$$

As a result, the screening length in PS regime is same as the ion sound radius i.e., $\rho_{sc} = \rho_s$.

The main results of this section are summarized in table(1).

Collisionality regimes	Screening length ρ_{sc}	Residual zonal flow $\frac{\phi_k(\infty)}{\phi_k(0)}$	B_θ-dependence
Banana regime	$= \sqrt{\rho_s^2 + \rho_\theta^2} \approx \rho_\theta$	$\approx \left(\frac{B_\theta}{B_T}\right)^2$	Favorable
Plateau regime	$= \sqrt{\rho_s^2 + \mathcal{L}\rho_\theta^2} \approx \mathcal{L}^{1/2}\rho_\theta$	$\approx \frac{1}{\mathcal{L}}\left(\frac{B_\theta}{B_T}\right)^2$	Favorable
Pfirsch-Schluter	$= \rho_s$	$= 1$	None

Table 1. Summary of results in all the three regimes of edge collisionality. $\mathcal{L}$ is defined in equation(24).

In summary, the screening lengths in the three regimes compare as $\rho_{sc}^{PS} \ll \rho_{sc}^{plateau} < \rho_{sc}^{banana}$, hence the residual zonal potential strengths compare as

$$\left(\frac{\phi_k(\infty)}{\phi_k(0)}\right)_{Pfirsch-Schluter} \gg \left(\frac{\phi_k(\infty)}{\phi_k(0)}\right)_{plateau} > \left(\frac{\phi_k(\infty)}{\phi_k(0)}\right)_{banana} \quad (40)$$

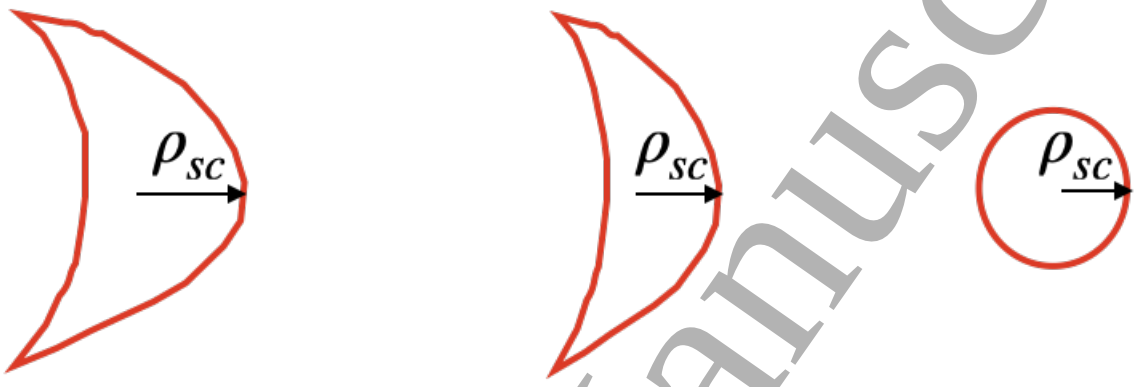

Figure 2. Cartoon of screening in banana(left), plateau(center), and PS regimes

Given the same damping and drive, zonal flow is thus strongest in PS regime. The poloidal field scaling of the zonal flow screening is lost there. The effective inertia is limited to a gyroradius by high collisionality, because neoclassical polarization vanishes in the PS regime. However, recent studies on the HL-2A tokamak suggest that the edge is more likely to be in the plateau regime [47]. Hence, in the following section, we utilize the plateau regime neoclassical polarization to obtain a novel drift wave zonal flow model.

3. Zonal flow- drift wave system with neoclassical polarization

In this section we develop the theory of the drift wave zonal flow system with neoclassical polarization. This is a well trodden subject. The new element here, and the goal of this section is to understand how neoclassical polarization modifies the feedback loop

structure for the system. The Laplace transformed quasineutrality equation reads as:

$$\varepsilon(p)\nabla^2\phi(p) = 4\pi\rho(p) \tag{41}$$

where $\varepsilon(p) = \varepsilon_{cl}(p) + \varepsilon_{nc}(p) = \frac{\omega_{pi}^2}{\omega_{ci}^2}\left\{1 + \frac{q^2}{\epsilon^2}\mathcal{L}\right\}$. Note that we ignored the frequency dependent contribution $\mathcal{P}(p)$ to the neoclassical polarization, since $\mathcal{P}(p) \to 0$ as $p = i\omega \to 0$ for the zonal mode. The inverse Laplace transform of the zonal component gives

$$\frac{\omega_{pi}^2}{\omega_{ci}^2}\left\{1 + \frac{q^2}{\epsilon^2}\mathcal{L}\right\}\left\langle\nabla^2\phi(t)\right\rangle = 4\pi\left\langle\rho(t)\right\rangle \tag{42}$$

where the angular bracket $\langle ...\rangle$ represents flux surface averaging. Taking the time derivative yields

$$\frac{\partial}{\partial t}\frac{\omega_{pi}^2}{\omega_{ci}^2}\left\{1 + \frac{q^2}{\epsilon^2}\mathcal{L}\right\}\left\langle\nabla^2\phi(t)\right\rangle = -4\pi\frac{\partial\langle J_r\rangle}{\partial r}, \tag{43}$$

so

$$\frac{\partial}{\partial t}\frac{\omega_{pi}^2}{\omega_{ci}^2}\left\{1 + \frac{q^2}{\epsilon^2}\mathcal{L}\right\}\left\langle\nabla^2\phi(t)\right\rangle = -4\pi e\int d^3v\left[S_i - S_e\right] \tag{44}$$

and

$$\frac{\partial}{\partial t}\left\{1 + \frac{q^2}{\epsilon^2}\mathcal{L}\right\}\left\langle\nabla^2\phi(t)\right\rangle = -\frac{\partial}{\partial r}\left\langle\delta v_{Er}\nabla_\perp^2\delta\phi\right\rangle. \tag{45}$$

where $S_{i,e} = \left\langle\delta\vec{v}_E\cdot\vec{\nabla}\delta f_{i,e}\right\rangle$. Here onwards, defining $\varepsilon = 1 + \frac{q^2}{\epsilon^2}\mathcal{L}$ and including viscous damping, the zonal vorticity evolution equation becomes

$$\frac{d}{dt}\varepsilon\left\langle\nabla_\perp^2\phi\right\rangle = -\frac{\partial}{\partial x}\left\langle\delta v_{Er}\nabla_\perp^2\delta\phi\right\rangle + \mu_0\nabla_\perp^2\left\langle\nabla_\perp^2\phi\right\rangle \tag{46}$$

where the first term on the right hand side is the divergence of vorticity flux. The equation(46) is in dimensional form. For simplicity, the potential fluctuation is assumed to be due to drift waves, governed by the Hasegawa - Wakatani model [52, 53]. The ions are assumed to be cold i.e., $T_i = 0$. Note that T_i-effects are not crucial to wave

dynamics, but are important to the physics of zonal flows. Hence we adopt the Hasegawa - Wakatani model.

$$\frac{d}{dt}\nabla_\perp^2\tilde{\phi} + \tilde{v}_E\cdot\vec{\nabla}\left\langle\nabla_\perp^2\tilde{\phi}\right\rangle = -\chi_e\nabla_\parallel^2\left(\tilde{\phi}-\tilde{n}\right) - \left\{\tilde{\phi},\nabla_\perp^2\tilde{\phi}\right\} + \mu\nabla_\perp^4\tilde{\phi} \quad (47)$$

$$\frac{d\tilde{n}}{dt} + \tilde{v}_E\cdot\frac{\vec{\nabla}\langle n\rangle}{\langle n\rangle} = -\chi_e\nabla_\parallel^2\left(\tilde{\phi}-\tilde{n}\right) - \left\{\tilde{\phi},\tilde{n}\right\} + D\nabla_\perp^2\tilde{n} \quad (48)$$

The above equations(47) and (48) have been written in dimensionless form. Potential and density are normalized as $\tilde{n} = \delta n/n$, $\tilde{\phi} = e\delta\phi/T_e$, respectively. Time and space are normalized as $t = \omega_{ci}t$, $x_\perp = x_\perp/\rho_s$. The normalized $E\times B$ velocity is $\tilde{v}_E = \frac{\delta v_E}{c_s} = \hat{z}\times\vec{\nabla}\tilde{\phi}$, $\chi_e = v_{te}^2/\nu_{ei}\Omega_i$ is electron parallel diffusivity, $v_{te} = \sqrt{2T_e/m_e}$ is electron thermal speed, μ is the normalized ion viscosity $\mu = \mu_0/\rho_s^2\Omega_i$ and D is the normalized collisional particle diffusivity $D = D_0/\rho_s^2\Omega_i$. The above equations describe the nonlinear evolution of vorticity fluctuation $\nabla_\perp^2\tilde{\phi}$ and density fluctuation $\tilde{n}$, which are coupled through parallel electron diffusivity χ_e. The parallel wave length is $k_\parallel \sim 1/\mathrm{qR}$, and perpendicular wavelength is $k_\perp\rho_s \sim 1$ so that $k_\parallel \ll k_\perp$ and the equations(47) and (48) describe a quasi-two-dimensional system. Defining the adiabaticity parameter $\alpha \equiv \chi_e k_\parallel^2/\omega_k$, the adiabatic regime correspond to $\alpha \gg 1$ and the hydrodynamic regime correspond to $\alpha \ll 1$. The set of equations(46), (47) and (48) constitute a self-consistent model for the coupled drift wave zonal flow system with neoclassical polarization effect. Linearized equations (47) and (48) support the dissipative drift wave dispersion relation:

$$k_\perp^2\omega_k^2 + i\omega_k\hat{\alpha}\left(1+k_\perp^2\right) - i\omega_{\star e}\hat{\alpha} = 0 \quad (49)$$

where $\hat{\alpha} = \chi_e k_\parallel^2 = \chi_e/q^2R^2$ and $\omega_{\star e} = (\rho_s/L_n)\,k_y$ is the drift frequency normalized by Ω_{ci}. Observe the q-dependence of the adiabaticity parameter via the parallel wave number. Notice that higher q (at fixed R) drive the system towards the hydrodynamic regime. The behavior of the Hasegawa - Wakatani model in different adiabaticity regimes is summarized in table(2).

Collisionality regimes ($\alpha \equiv \chi_e k_\parallel^2/\omega_k$)	$\tilde{n}$ and $\tilde{\phi}$ correlation	vorticity eqn(47)	density eqn(48)	Linear eigen values
adiabatic , $\alpha \gg 1$	$\tilde{n} \approx \tilde{\phi}$, strong correlation	Hasegawa-Mima equation [54].		$\omega_{rk} = \omega_{\star e}/\left(1+k_\perp^2\right)$ $\gamma_k = k_\perp^2 \omega_{rk}^2/\hat{\alpha}\left(1+k_\perp^2\right)$
hydrodynamic, $\alpha \ll 1$	weak correlation	2D Navier-Stokes	Passive scaler	$\omega_{rk} = sign(k_y)\gamma_k$ $\gamma_k = \left(\hat{\alpha}\left\|\omega_{\star e}\right\|/2k_\perp^2\right)^{1/2}$

Table 2. Behavior of Hasegawa - Wakatani model in adiabatic and hydrodynamic regimes.

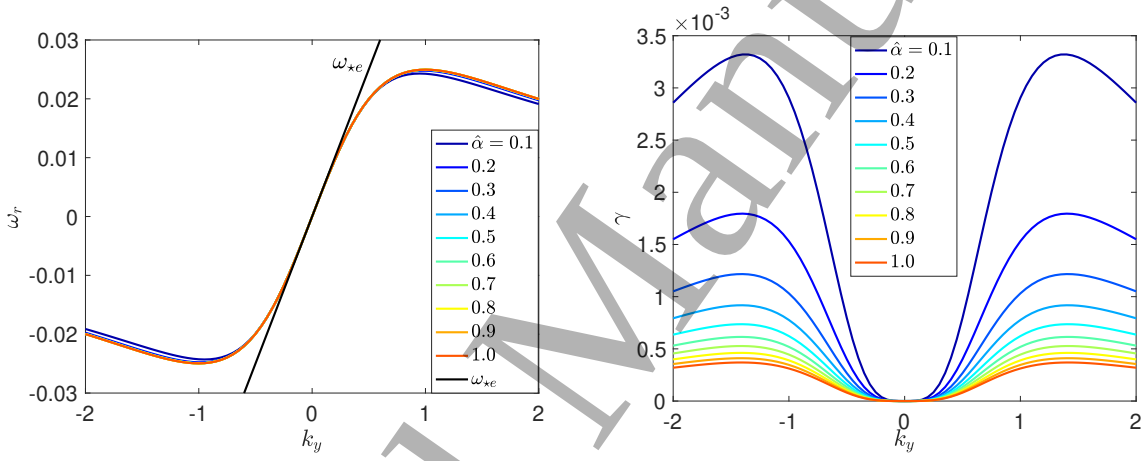

Figure 3. Real frequency and growth rate in the adiabatic regime, obtained from numerical solutions of equation(49). The growth rate drops with $\hat{\alpha}$ while real frequency remains almost independent on $\hat{\alpha}$.

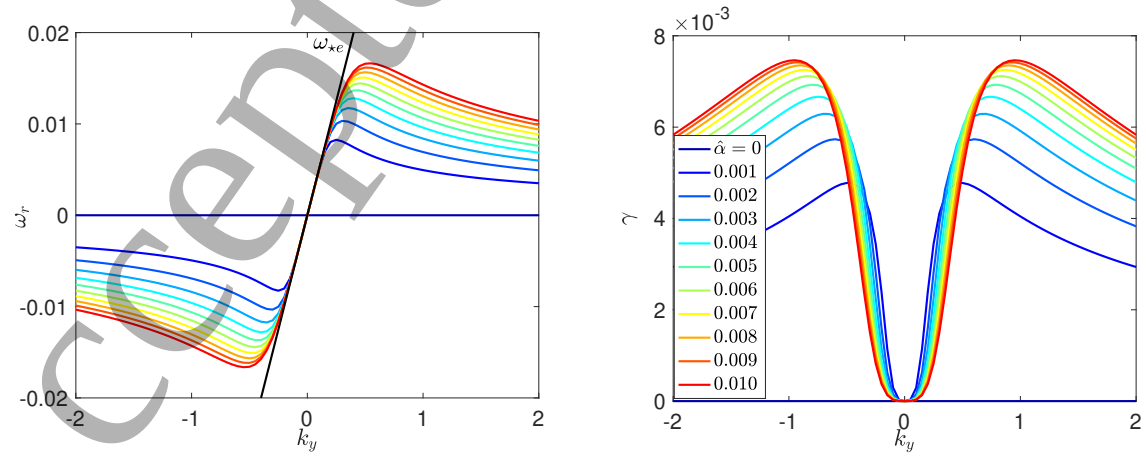

Figure 4. Real frequency and growth rates in the hydro regime, obtained from numerical solutions of equation(49). Both real frequency and growth rate increases with $\hat{\alpha}$.

The numerical solutions of the dispersion relation equation(49) in the adiabatic and hydro regime are plotted in figures(3) and (4), respectively. Notice that in adiabatic regime, $\omega_{rk} \sim \hat{\alpha}^0$, $\gamma_k \sim 1/\hat{\alpha}$. On the other hand, in hydro regime $\omega_{rk} = \gamma_k \sim \hat{\alpha}^{1/2}$.

4. Poloidal field dependence in zonal intensity

Here we study the poloidal field dependence of modulational growth and zonal polarization noise in the spectral evolution of zonal intensity. The aim here is to understand how consideration of neoclassical polarization modifies existing theoretical results. To start, the H-W system in spectral form reads

$$\left(\frac{\partial}{\partial t} + \mu k_\perp^2 + \frac{\hat{\alpha}_k}{k_\perp^2}\right) k_\perp^2 \phi_k - \hat{\alpha}_k n_k = \frac{1}{2} \sum_{\vec{p}+\vec{q}=\vec{k}} \hat{z} \cdot \vec{p} \times \vec{q} \left(q^2 - p^2\right) \phi_p \phi_q \tag{50}$$

$$\left(\frac{\partial}{\partial t} + \hat{\alpha}_k\right) n_k + \left(-\hat{\alpha}_k + i\omega_{\star e}\right) \phi_k = \frac{1}{2} \sum_{\vec{p}+\vec{q}=\vec{k}} \hat{z} \cdot \vec{p} \times \vec{q} (\phi_p n_q - \phi_q n_p) \tag{51}$$

For this two field drift wave turbulence model, the conserved (ideal) quantities are kinetic energy $E = \sum_k E_k = \sum_k \frac{1}{2} k^2 |\phi_k|^2$ and fluid enstrophy $Z = \sum_k Z_k = \sum_k \frac{1}{2} k^4 |\phi_k|^2$, the internal energy $E_n = \sum_k E_{nk} = \sum_k \frac{1}{2} |n_k|^2$ and the cross-correlation $C = \langle n \nabla_\perp^2 \phi \rangle = \sum_k k_\perp^2 n \phi_k^\star$. A detailed study of the coupled evolution of kinetic energy, internal energy and cross correlation spectra has been discussed recently in Ref [48]. Here we focus only on how neoclassical polarization modifies the spectral evolution of zonal kinetic energy spectra. The evolution equation for the kinetic energy spectra is obtained by multiplying the equation(50) by $\phi_k^\star$ and adding the resulting equation with the conjugate of equation(50) multiplied by ϕ_k. Taking statistical average (denoted by the angular bracket $\langle\rangle$) of the resulting equation yields an energy equation (equation(17) of Ref [48]).

For the zonal mode $k_y = k_\parallel = 0$, so the zonal kinetic energy spectrum equation becomes:

$$\left(\frac{\partial}{\partial t} + \mu k_\perp^2\right) \varepsilon k_\perp^2 \left\langle |\phi_k|^2 \right\rangle = \Re \sum_{\vec{k}=\vec{p}+\vec{q}} \hat{z} \cdot \vec{p} \times \vec{q} \left(q^2 - p^2\right) \left\langle \phi_k^\star \phi_p \phi_q \right\rangle \tag{52}$$

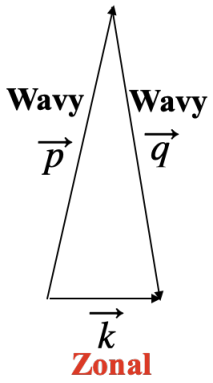

Figure 5. Geometry of wave interaction triad such that $\vec{k} = \vec{p} + \vec{q}$. The small leg $\vec{k}$ is the zonal mode.

Energy in the zonal wave number $\vec{k}$ is fed by the momentum conserving triad interactions, as shown in figure(5). The zonal kinetic energy is determined by the triple correlation of zonal mode potential ϕ_k with the wavy mode potentials ϕ_p and ϕ_q. The triplet correlations $\langle \phi_k^\star \phi_p \phi_q \rangle$, appearing on the right hand side of equation(52), are determined by the phase coherency among the three modes $\vec{k}$, $\vec{p}$, $\vec{q}$. Triad interactions are approximated using standard closure theory methods. These are discussed in detail in Ref [48]. The interactions can be identified as incoherent emission or coherent interaction. Then the incoherent emission part of the triad correlation is:

$$\left\langle \delta\phi_k^\star \phi_p \phi_q \right\rangle = \Theta_{kpq} \frac{1}{\varepsilon k_r^2} \hat{z} \cdot \vec{p} \times \vec{q} \left(q^2 - p^2\right) \left\langle |\phi_p|^2 \right\rangle \left\langle |\phi_q|^2 \right\rangle \tag{53}$$

where the triad interaction time is

$$\Theta_{kpq} = \frac{1}{i\left(\omega_p + \omega_q\right) + \eta_k + \eta_p + \eta_q} \tag{54}$$

Notice that ω is the linear (complex) frequency and η is the nonlinear damping rate of

turbulence. Similarly, the coherent part of the triad correlation is:

$$\begin{aligned}\left\langle \phi_k^\star \delta\phi_p \phi_q \right\rangle &= \Theta_{kpq} \left(\hat{z}\cdot\vec{p}\times\vec{q}\right) a_p \left(k^2-q^2\right) \left\langle |\phi_q|^2 \right\rangle \left\langle |\phi_k|^2 \right\rangle \\ &+ \Theta_{kpq} \left(\hat{z}\cdot\vec{p}\times\vec{q}\right) b_p \left(\left\langle |\phi_q|^2 \right\rangle \left\langle n_k \phi_k^\star \right\rangle - \left\langle |\phi_k|^2 \right\rangle \left\langle n_q^\star \phi_q \right\rangle \right) \end{aligned} \quad (55)$$

The coupling coefficients a_p and b_p are

$$a_p = \left(1 - \frac{i\omega_p}{\hat{\alpha}_p}\right) b_p; \qquad b_p = \frac{1}{det(A_p)} \quad (56)$$

where ω_p is the frequency of the linear eigenmode and $det(A_p)$ is given by

$$det(A_p) = \sqrt{\left(1+p^2\right)^2 - 4i\omega_{\star e}\left(\frac{p^2}{\hat{\alpha}_p}\right)} \quad (57)$$

Hence, the zonal spectral intensity equation becomes:

$$\left(\frac{\partial}{\partial t} + 2\mu k_x^2\right) \left\langle |\phi_k|^2 \right\rangle + 2\eta_{1k} \left\langle |\phi_k|^2 \right\rangle + \Re\left[2\eta_{2k} \left\langle n_k \phi_k^\star \right\rangle\right] = F_{\phi k} \quad (58)$$

In the above equation(58), the second term on the left, proportional to zonal intensity, represents nonlinear damping of the zonal mode. The damping rate is:

$$\eta_{1k} = -\Re \sum_{\vec{k}=\vec{p}+\vec{q}} \frac{1}{\varepsilon k_x^2} \left(\hat{z}\cdot\vec{p}\times\vec{q}\right)^2 \left(q^2-p^2\right) \Theta_{kpq} \left[a_p \left(k^2-q^2\right) - b_p \frac{\left\langle n_q^\star \phi_q \right\rangle}{\left\langle |\phi_q|^2 \right\rangle} \right] \left\langle |\phi_q|^2 \right\rangle \quad (59)$$

The third term on the left hand side of equation(58) includes coupling to zonal cross correlation $\langle n_k \phi_k^\star \rangle$ with the cross coupling coefficient given by

$$\eta_{2k} = -\sum_{\vec{k}=\vec{p}+\vec{q}} \frac{1}{\varepsilon k_x^2} \left(\hat{z}\cdot\vec{p}\times\vec{q}\right)^2 \left(q^2-p^2\right) \Theta_{kpq} b_p \left\langle |\phi_q|^2 \right\rangle . \quad (60)$$

Finally, the term on the right hand side is the zonal nonlinear noise/ polarization noise:

$$F_{\phi k} = \Re \sum_{\vec{k}=\vec{p}+\vec{q}} \frac{1}{\left(\varepsilon k_r^2\right)^2} \left(\hat{z}\cdot\vec{p}\times\vec{q}\right)^2 \left(q^2-p^2\right)^2 \Theta_{kpq} \left\langle |\phi_p|^2 \right\rangle \left\langle |\phi_q|^2 \right\rangle \quad (61)$$

Note that the zonal noise term here is exactly the same as the zonal noise term for the Hasegawa-Mima equation, and is always positive definite. It is determined by the advection of vorticity. However, the eddy damping term is different from that for the

Hasegawa-Mima case, due to non-adiabaticity of electrons. This is discussed in Ref [48] and we do not repeat it here. Only the adiabatic regime ($\alpha > 1$) is considered. Using $k^2 \ll q^2$ and expanding around $\vec{p} = -\vec{q}$, the nonlinear damping rate becomes:

$$\eta_{1k} = \sum_{\vec{q}} \frac{k_x^2 q_y^2}{\varepsilon} \Theta^{(r)}_{k,-q,q} q_x \frac{\partial}{\partial q_x} \left[\left(a_{-q} q^2 + b_{-q} R_q^\star \right)^{(r)} I_q \right] \tag{62}$$

Thus, nonlinear damping rate of the zonal flow scales with poloidal field as $\eta_{1k} \sim \varepsilon^{-1} \sim B_\theta^2$. Since, $\Re \left[\eta_{2k} \left\langle n_k \phi_k^\star \right\rangle \right] = \eta_{2k}^{(r)} \Re \left\langle n_k \phi_k^\star \right\rangle - \eta_{2k}^{(i)} \Im \left\langle n_k \phi_k^\star \right\rangle$, one needs to evaluate both real and imaginary parts of the cross-coefficient η_{2k}. Using the expansion procedure outlined above, the real part of η_{2k} becomes

$$\eta_{2k}^{(r)} = -\sum_{\vec{q}} \frac{k_x^2 q_y^2}{\varepsilon} \Theta^{(r)}_{k,-q,q} q_x \frac{\partial}{\partial q_x} \left[b_{-q}^{(r)} I_q \right] \tag{63}$$

and the imaginary part becomes

$$\eta_{2k}^{(i)} = -\sum_{\vec{q}} \frac{k_x^2 q_y^2}{\varepsilon} \Theta^{(r)}_{k,-q,q} q_x \frac{\partial}{\partial q_x} \left[b_{-q}^{(i)} I_q \right] = 0 \tag{64}$$

Note that $\eta_{2k}^{(i)} = 0$ due to the q_y-symmetry of $b_q^{(i)}$- i.e., it is odd in q_y. This means that only $\Re \left\langle n_k \phi_k^\star \right\rangle$-i.e., the real part of the zonal cross-spectrum, affects the evolution of zonal intensity. Thus the cross-transfer rate scales with current $\eta_{2k}^{(r)} \sim \varepsilon^{-1} \sim B_\theta^2$. Similarly the zonal noise term can be reduced to

$$\begin{aligned} F_{\phi k} &= \sum_q \frac{4}{\varepsilon^2} q_y^2 q_x^2 \Theta^{(r)}_{k,-q,q} I_{-q}(t) I_q(t) + \mathcal{O}(k_r^2/q_r^2) \\ &\approx \frac{4}{\varepsilon^2} \sum_q \Pi_q^2 \Theta^{(r)}_{k,-q,q} \end{aligned} \tag{65}$$

where $\Pi_q = q_y q_r I_q$ is the spectral form of Reynolds stress. The nonlinear zonal noise scales with current as $F_{\phi k} \sim \varepsilon^{-2} \sim B_\theta^4$. Notice that zonal noise has stronger B_θ scaling than the modulational growth rate.

For the relevant adiabatic regime $\omega_q < \hat{\alpha}_q$, the linear density - potential response

function, can be reduced to

$$R_{nq} = \left(1 - i\frac{\omega_{\star e}}{\hat{\alpha}_q}\right)\left(1 - i\frac{\omega}{\hat{\alpha}_q}\right)^{-1} = 1 + \frac{q_\perp^4}{1+q_\perp^2}\frac{1}{\alpha_q^2} - \frac{iq_\perp^2}{\alpha_q} + \mathcal{O}\left(\frac{1}{\alpha_q^3}\right) \tag{66}$$

The coupling parameters in the adiabatic regime become

$$a_q = \left(1 - \frac{i}{\alpha_q} + \frac{1}{1+q^2}\frac{q_\perp^2}{\alpha_q^2}\right) b_q \tag{67}$$

$$b_q = \frac{1}{1+q^2}\left(1 + i\frac{2}{1+q^2}\frac{q^2}{\alpha_q}\right) + \mathcal{O}\left(\frac{1}{\alpha_q^2}\right) \tag{68}$$

. Using the expression for R_q in the adiabatic regime, the nonlinear zonal damping rate becomes

$$\eta_{1k}^{zonal} = \sum_q \frac{k_x^2 q_y^2}{\varepsilon}\Theta_{k,-q,q}^{(r)} q_x \frac{\partial}{\partial q_x}\left[\left(1 - \frac{2q_\perp^4}{\left(1+q_\perp^2\right)^2}\frac{1}{\alpha_q^2}\right) I_q\right] \tag{69}$$

This shows that the nonlinear damping of zonal flow is negative when the turbulence intensity spectrum satisfies $\frac{\partial I_q}{\partial q_r} < 0$, which is usually the case. In this case, 'negative viscosity' results -i.e., $\eta_{1k}^{(r)} < 0$ and $\sim k_x^2$, symptomatic of transfer to large scales. The total growth $\mathcal{G}_k$ of zonal flows is determined by $\eta_{1k}^{(r)}$ and the linear damping μk_x^2, so, $\mathcal{G}_k = -\eta_{1k} - \mu k_x^2$. $\mathcal{G}_k$ defines a critical spectral slope for marginality to modulational instability. It is also clear that the zonal growth rate is maximal for the strongly adiabatic regime, when $\alpha_q \to \infty$. This suggests that non-adiabatic density fluctuations inhibit the inverse transfer of energy to zonal flows.

The cross-coefficient $\eta_{2k}^{(r)}$ is independent of α since $b_q^{(r)}$ (from equation(68)) is independent of α. Hence, $\eta_{2k}^{(r)}$ is always positive for negative spectral slope. This means that the zonal cross correlation can cause either forward or inverse transfer of energy, depending on the sign of the cross-correlation $\langle n_k \phi_k^\star \rangle$(the relative phase between zonal density and potential).

A straightforward but tedious calculation of $\langle n_k \phi_k^\star \rangle$ shows that the real part of the zonal cross-spectrum $\Re \langle n_k \phi_k^\star \rangle < 0$ [48]. Since $\eta_{2k}^{(r)} > 0$, this means that, $\Re \langle n_k \phi_k^\star \rangle$ adds to growth of zonal intensity i.e., the backward transfer of turbulent kinetic energy.

5. Shear layer collapse: Physics, Critical scalings and Consequences

Here we determine the conditions for zonal flow collapse, as predicted by a simple predator prey model which evolves turbulence and zonal flow energy. This is appropriate to the L-mode edge, where ∇P is weak, so diamagnetic electric fields are negligible. For this purpose, we follow the predator - prey model of Ref [48], which evolves turbulence energy E_t and zonal flow energy E_v in 0D. The turbulence energy E_t evolves as

$$\frac{\partial E_t}{\partial t} = \gamma E_t - \sigma E_v E_t - \eta E_t^2. \tag{70}$$

The first term on the right hand side represents linear growth of turbulence, with growth rate γ. The second term represents turbulence damping due to shearing - i.e., scattering in k_x-space induced by the zonal flow shearing field, approximated as stochastic. The third term represents the nonlinear damping of turbulence, by self-interaction - i.e., nonlinear transfer to dissipation. The zonal flow energy E_v evolves as

$$\frac{\partial E_v}{\partial t} = \sigma E_t E_v - \gamma_d E_v + \beta E_t^2 \tag{71}$$

where the first term on the right hand side represents modulational growth of zonal flow. This necessarily conserves energy against the second term in equation(70) - i.e., stochastic straining of turbulent eddies results in energy transfer to zonal flows. The second term on the RHS of equation(71) represents damping of zonal flow by viscous, ionization and charge exchange friction, with total damping rate γ_d. The

third term βE_t^2 on the right hand side of equation (71) represents drive by zonal noise, as discussed in Ref [48]. Equations(70) and (71) are normalized as follows: $t \equiv t\Omega_i$, $\gamma \equiv \gamma/\Omega_i$, $\sigma \equiv \sigma/\Omega_i$, $\gamma_d \equiv \gamma_d/\Omega_i$, $\eta \equiv \eta/\Omega_i$, $\beta \equiv \beta/\Omega_i$, $E_t = q_y^2 \left|e\phi_q/T_e\right|^2$, $E_v = k_x^2 \left|e\phi_k/T_e\right|^2$, $k_x \equiv k_x\rho_s$ and $q_y \equiv q_y\rho_s$. The parameters of this model are the normalized linear growth rate $\gamma = \left(q_\perp^2/\hat{\alpha}\right)\omega_{\star e}^2/\left(1+q_\perp^2\right)^3$ for the (usually relevant) adiabatic regime, where $\hat{\alpha} = q_\parallel^2 v_{te}^2/\nu_{ei}\Omega_i$ is the adiabaticity parameter, normalized zonal growth coefficient $\sigma = \sum_q (2/\varepsilon)\, k_x^2 \Theta_{k,-q,q}^{(r)}$, normalized zonal noise coupling parameter $\beta = \sum_q (4/\varepsilon^2)\, k_x^2 q_y^{-2} q_x^2 \Theta_{k,-q,q}^{(r)}$. The normalized nonlinear damping rate is $\eta \approx \sum_q q^2 \Theta_{k,p,q}^{(r)}$. Nonlinear damping (or eddy damping) results from the phase coherent part of the triplet correlation $\langle \phi_k^\star \phi_p \phi_q \rangle$ emerging as a consequence of the momentum conserving triad interaction in the turbulent kinetic energy equation [48]. Here Θ is the normalized triad interaction time, defined in equation(54). For simplicity, Θ can be approximated as the wave correlation time $\tau_c \gtrsim \omega_{\star e}^{-1}$. The zonal flow damping rate γ_d is the sum of viscous (collisional) and ionization and charge exchange damping rates, and is given by :

$$\gamma_d = \gamma_{visc} + \gamma_{icx} = \mu k_x^2 + \left(\langle \nu\sigma \rangle_i + \langle \nu\sigma \rangle_{cx}\right) n_n/\Omega_i = \frac{\rho_i^2 \nu_{ii}}{\rho_s^2 \Omega_i} k_x^2 + \left(\langle \nu\sigma \rangle_i + \langle \nu\sigma \rangle_{cx}\right) n_n/\Omega_i \quad (72)$$

Notice that viscous damping depends on ion density as well as the wave number of the zonal flow k_x. Ionization and charge exchange damping are independent of ion density, and scale free. The zonal flow is a mesoscopic mode, with radial scale l_z lying between the ion larmor radius (microscale) and system size (macroscale). Frequently, one takes $l_z \approxeq \sqrt{\rho_s L_n} \sim 10\rho_s - 30\rho_s$ as an approximate zonal flow scale. This is true for PS regime where screening length is same as the ion sound radius i.e., $\rho_s = \rho_{sc}$. This suggests that $l_z \sim \sqrt{\rho_{sc} L_n}$, in general. Since $\rho_{sc}^{PS} \ll \rho_{sc}^{plateau} < \rho_{sc}^{banana}$, this implies $l_z^{PS} \ll l_z^{plateau} < l_z^{banana}$. The neoclassical polarization dependence of the parameters ($\sigma \sim \varepsilon^{-1} \sim B_\theta$ and $\beta \sim \varepsilon^{-2} \sim B_\theta^2$) makes this model suitable for study of the scalings of

zonal collapse. It differs from previous incarnations of this family of shear flow transition models [55].

The above equations(70) and (71) yield, for steady state:

$$\sigma E_v = \gamma - \eta E_t \tag{73}$$

and

$$\left(\sigma\varepsilon - \gamma_d\right) E_v + \beta E_t^2 = 0 \tag{74}$$

Defining $E_{t1} = \gamma_d/\sigma$ and $E_{t2} = \gamma/\eta$ and using the above equations, the fixed points follow from the roots of :

$$\left(1 - \frac{\beta}{\eta}\right) E_t^2 - E_t \left(E_{t1} + E_{t2}\right) + E_{t1} E_{t2} = 0. \tag{75}$$

These are:

$$E_t^{\pm} = \frac{\left(E_{t1} + E_{t2}\right) \pm \sqrt{\left(E_{t1} + E_{t2}\right)^2 - 4\left(1 - \frac{\beta}{\eta}\right) E_{t1} E_{t2}}}{2\left(1 - \frac{\beta}{\eta}\right)} \tag{76}$$

The corresponding zonal flow energies are

$$E_v^{\pm} = \sigma^{-1}\left(\gamma - \eta E_t^{\pm}\right) \tag{77}$$

Note that for the case without noise ($\beta = 0$), $E_{t0}^{+} = E_{t2}$, $E_{t0}^{-} = E_{t1}$, $E_{v0}^{+} = 0$ and $E_{v0}^{-} = \sigma^{-1}\eta\left(E_{t2} - E_{t1}\right)$. It is straightforward to show that the fixed point $\left(E_{t0}^{-}, E_{v0}^{-}\right) = \left(E_{t1}, \sigma^{-1}\eta\left(E_{t2} - E_{t1}\right)\right)$ is stable.

There is a clear threshold (in growth rate γ) for excitation of zonal flow in the noise free case. The threshold reflects the fact that a critical level of turbulence intensity is required to overcome the flow damping, so as to induce modulational instability. This is consistent with numerical solutions, plotted in Figure(6). The phase plane in Figure (6) is obtained by performing a linear growth rate scan, with noise strength as a parameter. The figure indeed shows that, without noise, there is a threshold in growth rate for appearance of stable zonal flows. This threshold is set by the contest between insta-

bility growth and flow damping, as mediated by fluctuation → flow energy coupling. Below the threshold, there is only turbulence, and no zonal flows. Above the threshold, turbulence and zonal flows co-exist. Upon ramping up the growth rate, but remaining below the threshold, the turbulence energy increases in proportion to γ/η , until it 'locks' at the threshold γ_d/σ. Beyond the threshold, turbulence energy remains fixed at the value γ_d/σ, while the zonal flow energy continues to increase as $\sigma^{-1}\eta\left(\gamma/\eta - \gamma_d/\sigma\right)$. Any free energy surplus beyond the threshold of turbulence growth (noting that growth $\gamma \sim \nabla n, \nabla T$ - the free energy) is channeled into the flow. In contrast, with noise, both zonal flow and turbulence co-exist at any value of the growth rate -i.e., there is no hard threshold for zonal flow excitation. Both zonal flow and turbulence energy increase with growth rate. In this case, zonal flow energy is related to turbulence energy by $E_v = \beta E_t^2/\left(\gamma_d - \sigma E_t\right)$. Note that with noise, the turbulence energy never actually hits the modulational instability threshold, absent noise! Significant zonal flows are generated well below the modulational instability threshold. This does not mean that the modulational growth of zonal flow is absent! Without noise, modulational growth requires an initial seed field (a non-zero initial condition). This initial seed is irrelevant to the growth of zonal flows with noise. Noise itself acts as a seed for the zonal flow growth. Note that without modulational growth, the saturated level of zonal flow will be lower, and so the turbulence level will be higher, than the values shown in Figure(6).

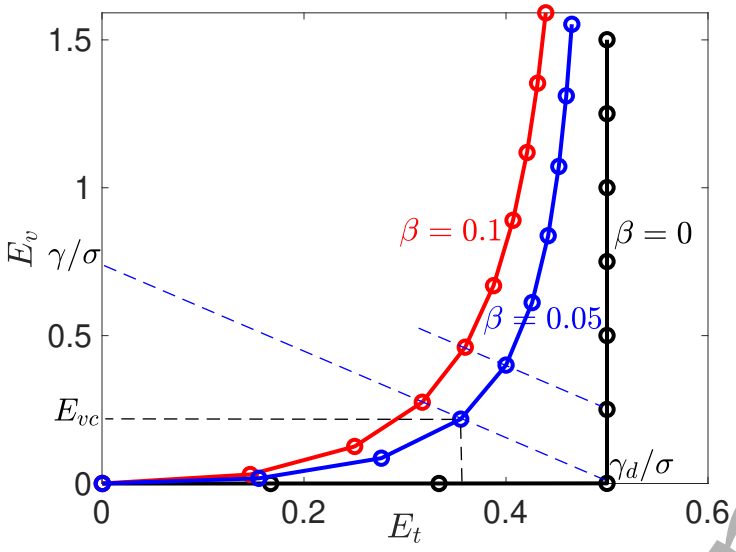

Figure 6. Zonal flow energy E_v vs turbulence energy E_t in a linear growth rate γ scan with noise strength β as a parameter.

The above analysis established that there is no hard threshold for zonal flow emergence with noise. Rather, as linear growth increases, there is a continuous evolution from a state of weak zonal flow shear to a state of strong zonal flow shear . This can be seen in figure(6), where the blue and red curves show the zonal flow energy and turbulence energy phase curves, with zonal noise present. We take zonal flow 'collapse' to mean this continuous evolution from high shear to low shear - i.e, collapse is seen as a 'soft' transition. This means that zonal flow decay occurs when the zonal flow energy falls below a critical value E_{vc} i.e.,

$$E_v < E_{vc} \tag{78}$$

Now, E_{vc} is simply the upshift of the zero zonal energy state induced by noise. Proceeding perturbatively (as in Ref [48]),

$$E_{vc} = \frac{\beta}{\eta}\frac{\eta}{\sigma}\frac{\left(E_{t0}^{-}\right)^2}{E_{t0}^{+} - E_{t0}^{-}} \tag{79}$$

and

$$E_v^{\pm} = E_{v0}^{\pm} \mp \frac{\beta}{\eta}\frac{\eta}{\sigma}\frac{\left(E_{t0}^{\pm}\right)^2}{E_{t0}^{+} - E_{t0}^{-}} + \mathcal{O}\left(\frac{\beta^2}{\eta^2}\right) \tag{80}$$

Hence,

$$E_v < E_{vc} \implies E_{v0}^{-} < 0 \tag{81}$$

This means that the criterion for zonal flow collapse with noise tracks that for collapse of zonal flow, as predicted by the noise-free predator - prey model.

Without noise, the criterion for stable zonal flow emergence is

$$E_{v0}^{-} > 0 \implies \sigma^{-1}\left(\gamma - \eta E_{t0}^{-}\right) > 0 \implies \gamma > \eta\frac{\gamma_d}{\sigma} \tag{82}$$

. This means that the criterion for zonal flow decay and collapse is:

$$E_{v0}^{-} < 0 \implies \gamma < \eta\frac{\gamma_d}{\sigma} \tag{83}$$

The inequality(82), which specifies the condition for zonal flow persistence, can be cast in the form

$$\begin{aligned} &\frac{q_\perp^2}{\hat{\alpha}}\frac{\omega_{\star e}^2}{\left(1+q_\perp^2\right)^3} > \eta\frac{\gamma_d}{\frac{2}{\varepsilon}k_x^2\Theta} \\ &\implies \frac{\rho_s}{\sqrt{\rho_{sc}L_n}} > \left[\frac{\eta}{\Omega_i}\frac{\gamma_d}{2k_x^2\rho_s^2\Theta\Omega_i^2}\frac{\hat{\alpha}}{q_\perp^2\rho_s^2}\frac{\left(1+q_\perp^2\rho_s^2\right)^3}{q_y^2\rho_s^2}\right]^{1/4} \end{aligned} \tag{84}$$

where ρ_{sc} is the zonal flow screening length, given by $\rho_{sc}^2 = \varepsilon\rho_s^2 = \rho_s^2 + \mathcal{L}\rho_\theta^2$, and discussed in Section(2). All quantities on the RHS of equation(84) have been written explicitly, in dimensional form. *This shows that zonal flows collapse when the dimensionless scale length ratio $\rho_s/\sqrt{\rho_{sc}L_n}$ falls below a critical value, determined by the zonal flow damping rate γ_d, turbulence nonlinear damping rate η, triad interaction time Θ and adiabaticity parameter $\hat{\alpha}$. Indeed, the ratio $\rho_s/\sqrt{\rho_{sc}L_n}$ emerges as the natural dimensionless parameter characterizing shear layer persistence. Crucially, note that*

smaller ρ_{sc} -i.e., higher B_θ enlarges the regime of ZF persistence. We note that the dimensionless ratio $\rho_s/\sqrt{\rho_{sc}L_n}$ is equally relevant for the core region, which lies in the Banana regime. There the screening length is set by the poloidal gyroradius - i.e., $\rho_{sc} \approx \rho_\theta$.

The density scale length can be determined by particle balance, in steady state, i.e.,

$$\begin{aligned} \frac{\partial}{\partial x}\left[-D\frac{\partial n}{\partial x}\right] &= \langle\nu\sigma\rangle_i n_n n \\ \Longrightarrow \frac{D}{L_n} &= \frac{S}{n} \end{aligned} \tag{85}$$

where $S = \int dx \langle\nu\sigma\rangle_i n_n n$ is the integrated particle source function. The later depends on the ionization cross section $\langle\nu\sigma\rangle_i$ and neutral density n_n. D is turbulent particle diffusivity. In the adiabatic regime, the imaginary part of the linear density - potential response function is $R_{nq}^{(i)} = -q_\perp^2/\alpha$. This yields the quasilinear particle diffusivity $D = c_s\rho_s q_\perp^2\rho_s^2 E_t/\hat{\alpha}\left(1+q_\perp^2\rho_s^2\right)$. Using the saturated level of turbulence kinetic energy $E_t = \gamma_d/\sigma$, (as given by the predator - prey model), the particle diffusivity (in dimensional form) becomes

$$D = c_s\rho_s \frac{q_\perp^2\rho_s^2}{\hat{\alpha}\left(1+q_\perp^2\rho_s^2\right)} \frac{\rho_{sc}^2}{\rho_s^2} \frac{\gamma_d}{2k_x^2\rho_s^2\Theta\Omega_i^2}. \tag{86}$$

Equation(86) shows that particle diffusivity decreases with poloidal field $D \sim \frac{\rho_{sc}^2}{\rho_s^2} \sim B_\theta^{-2}$, since zonal flow shears intensify for weaker screening. Using the particle balance equation(85), the zonal flow persistence criterion(84) becomes,

$$\frac{S}{nc_s} > \frac{\rho_{sc}^3}{\rho_s^3}\left[\frac{\eta}{\Omega_i}\right]^{1/2}\left[\frac{\gamma_d}{2k_x^2\rho_s^2\Theta\Omega_i^2}\right]^{3/2}\left[\frac{q_\perp^2\rho_s^2}{\hat{\alpha}}\right]^{1/2}\left[\frac{\left(1+q_\perp^2\rho_s^2\right)}{q_y^2\rho_s^2}\right]^{1/2} \tag{87}$$

Inequality(87) gives the criterion for collapse of zonal flows, based on particle source strength. Zonal flows will collapse when the particle source strength falls below a critical value S_{crit}, which is determined by η, γ_d, and $\hat{\alpha}$. Inequality(87) also shows that the critical particle source strength S_{crit} scales with poloidal field as $S_{crit} \sim \frac{\rho_{sc}^3}{\rho_s^3} \sim B_\theta^{-3}$.

That is, the critical particle source strength decreases for stronger poloidal field(i.e., plasma current). Note that, in terms of particle diffusivity, the critical particle source increases with diffusivity and scales as $S_{crit} \sim D^{1/2}$. The origin of S_{crit} is consistent with the fact that collisional driftwave turbulence is ∇n - driven.

Inequality(87) may be converted to a limit on local edge density, in the region of the shear layer. Since $\hat{\alpha} \sim 1/n$, $\gamma_d = \gamma_{visc} + \gamma_{icx}$ where, $\gamma_{visc} \sim n$ and $\gamma_{icx} \sim n^0$, the above inequality leads to a seventh order polynomial in n. This is simplified if we consider separate limiting cases of $\gamma_d = \gamma_{visc}$ and $\gamma_d = \gamma_{icx}$. So for $\gamma_d = \gamma_{visc}$, we obtain the allowed density range for zonal flows persistence:

$$n < \frac{\rho_s}{\rho_{sc}} \left(\frac{S}{c_s}\right)^{1/3} \left(\frac{n\hat{\alpha}}{q_\perp^2 \rho_s^2}\right)^{1/6} \left[\frac{2\Theta\Omega_i^2}{\rho_i^2 \nu_{ii}/\rho_s^2 n}\right]^{1/2} \left[\frac{\Omega_i}{\eta}\right]^{1/6} \left[\frac{q_y^2 \rho_s^2}{(1+q_\perp^2\rho_s^2)}\right]^{1/6} \quad (88)$$

Inequality(88) gives the criterion for zonal flow collapse, in the form of a limit on the local edge density n. We see that zonal flows collapse when the local density exceeds a critical density n_{crit}, which scales with poloidal magnetic field as $n_{crit} \sim \frac{\rho_s}{\rho_{sc}} \sim B_\theta$. When $\gamma_d = \gamma_{icx}$, then

$$n < \frac{\rho_s^2}{\rho_{sc}^2} \left(\frac{S}{c_s}\right)^{2/3} \left(\frac{n\hat{\alpha}}{q_\perp^2 \rho_s^2}\right)^{1/3} \left[\frac{2k_x^2 \rho_s^2 \Theta \Omega_i^2}{\gamma_{icx}}\right] \left[\frac{\Omega_i}{\eta}\right]^{1/3} \left[\frac{q_y^2 \rho_s^2}{(1+q_\perp^2\rho_s^2)}\right]^{1/3} \quad (89)$$

gives the allowed density range. So, when the zonal flow damping is due to ionization and charge exchange friction, the poloidal field scaling of the critical local density for zonal flow collapse is somewhat stronger than for the case when the damping is viscous i.e., $n_{crit} \sim \frac{\rho_s^2}{\rho_{sc}^2} \sim B_\theta^2$.

What happens when the density exceeds the critical density? Well, zonal flows collapse and the turbulence level increases. As a result, the local edge particle and heat diffusivities increase. The edge density n_{edge} and temperature T_{edge} are related to particle

diffusivity D and heat diffusivity χ as

$$n_{edge} \approx l_z \frac{S_{eff}}{D} \tag{90}$$

and

$$T_{edge} \approx l_z \frac{Q}{n_{edge}\chi}. \tag{91}$$

Here $S_{eff} = \int_{a-\Delta r}^{a} dr \langle \nu\sigma \rangle_i n_n n_i$ is the particle source strength integrated over the (narrow) edge ionization layer Δr, Q is the heat flux from the core and l_z is scale of shear layer at the edge. D and χ necessarily increase upon collapse of zonal flows. As a result, the edge density and edge temperature decrease for fixed sources. These reductions are a consequence of a transport bifurcation - i.e., a 'back transition' from a state where the shear layer coexists with turbulence, to one with no shear layer. The power loss rate due to impurity radiation is given by $L = \sum_Z n n_Z L_Z(T_e)$, where n_Z is impurity density and $L_z(T_e)$ cooling rate of impurity species Z. Reduction of T_{edge} results in a increase in the power loss due to impurity radiation from low Z impurities (e.g. carbon). Hence, zonal flow collapse can lead to edge cooling by a sequence of shear layer collapse $\rightarrow$ increased edge transport $\rightarrow$ edge cooling $\rightarrow$ onset of radiative condensation and/or radiation - induced island growth. Note that, in this scenario, the radiative cooling is secondary (i.e., a consequence of) to the transport bifurcation. Further increase of edge density by increasing S_{eff} by intense neutral gas fueling at the edge (at fixed heating power) will cause edge cooling. Sufficiently strong cooling may trigger a MARFE [35] and or a radiation driven magnetic island [36, 56, 57], which can ultimately lead to disruption. In this way, we see that a transport bifurcation -i.e., edge shear layer collapse may trigger undesired macroscopic phenomena in the discharge, as schematized in figure(7).

Finally, we would like to emphasize that the zonal flow collapse criteria obtained here is

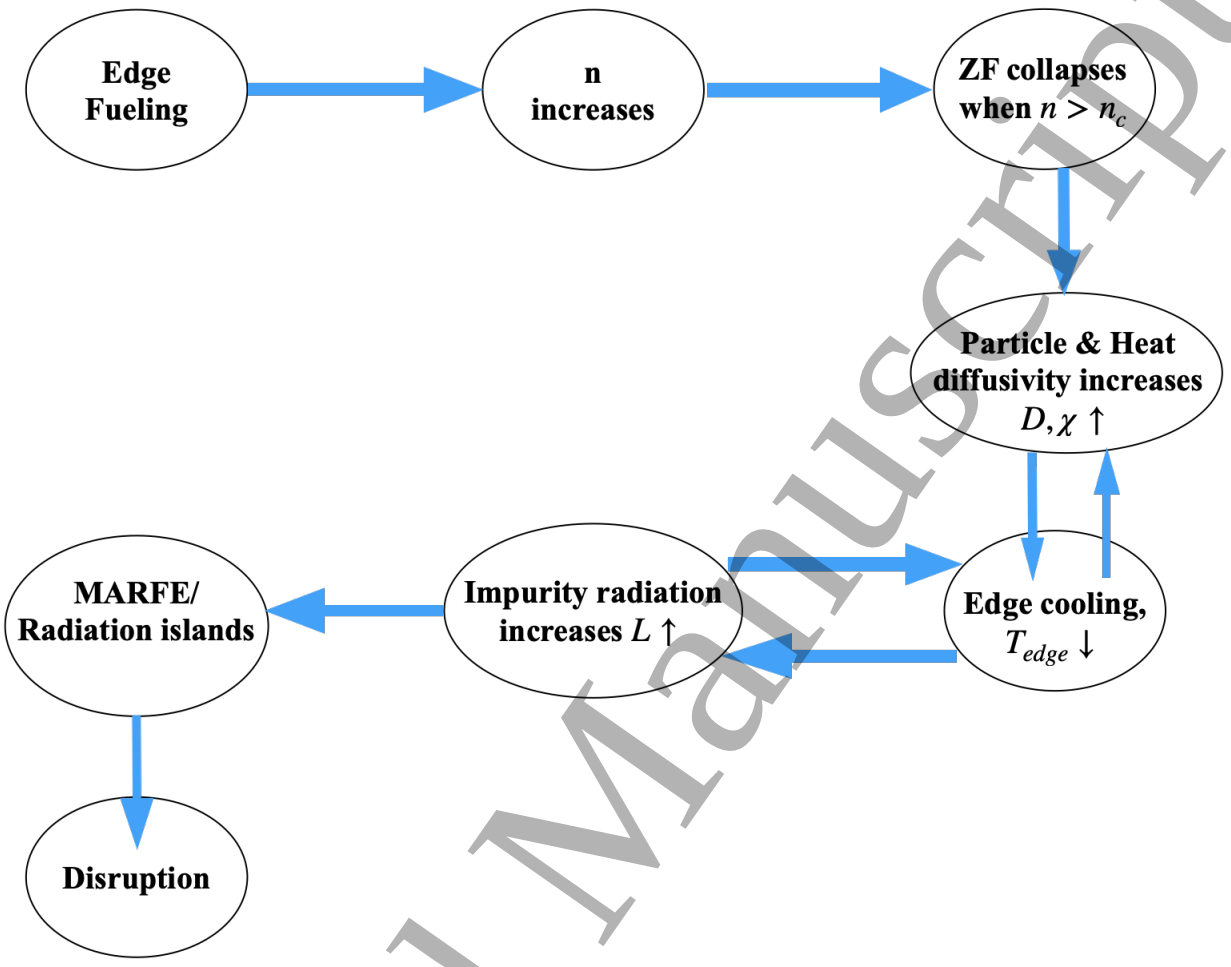

Figure 7. Enhanced transport due to zonal flow collapse can aggravate excitation of MARFE or radiation driven islands due to enhanced edge cooling, which can lead to disruption of discharge.

valid for the adiabatic regime i.e., $\alpha > 1$. Note that, $\alpha > 1$ is the regime of relevance for present-day tokamak edges. This is different from the zonal vorticity collapse predicted for the hydrodynamic regime ($\alpha < 1$) by R. Hajjar *et al* [40]. For $\alpha < 1$, quasilinear analysis reveals that the particle flux scales as $\Gamma_n \sim 1/\sqrt{\hat{\alpha}}$ and vorticity diffusivity scales as $\chi \sim 1/\sqrt{\hat{\alpha}}$. This means that the particle flux and the turbulent viscosity increase when $\alpha \ll 1$. Physically, in adiabatic regime, the wave energy flux is correlated with wave momentum flux such that the outgoing wave energy flux corresponds to incoming wave momentum flux, which naturally leads to the formation of zonal bands. This link of wave energy flux to Reynolds stress is broken in the hydro regime. As a result, zonal

flow production drops, turbulence is not effectively regulated and anomalous transport increases. This scenario is relevant in the event of the edge entering the hydrodynamic limit. Indeed, recent experiments [38] have identified correlation between shear layer degradation, Reynolds power decrease, particle flux increase and the $\alpha < 1$ regime.

The conclusions drawn in this section follow from the envelope equations(70) and (71). There are a number of experiments and simulations which support ("validate") these envelope equations. The earliest and the most notable one is a simulation of negative compressibility - driven turbulence [58]. For that, the turbulence intensity obtained by numerical simulations is compared with the predictions of the envelope equations. In particular, the predicted scaling of fluctuation intensity with zonal flow damping is recovered. Also, an experiment on DIII-D on the role of zonal flow predator-prey oscillations in triggering the transition to H-mode confinement [8] yields results consistent with the predictions of the extended(3-field) predator-prey model including pressure dynamics. Global gyrokinetic simulations [59] of ITG turbulence give a turbulent heat diffusivity proportional to ion-ion collisionality -i.e., zonal flow damping. This is in accord with the predictions (of turbulence intensity proportional to zonal flow damping) from the envelope equations(70) and (71).

6. Conclusions and discussions

In this paper, we have studied the physics of edge shear collapse and its role in the approach to the Greenwald density limit . The study was motivated by the classic observation that shallow pellet injection - which avoids excessive edge cooling - provokes, 'soft', transport driven relaxation to the density limit rather than the familiar MARFES and disruption [27]. It suggests that the Greenwald limit emerges from particle transport physics. Recent experiment supported this long - standing hypothesis with the finding

that as $n \to n_G$, edge zonal flow Reynolds power density drops, thus degrading ZF production, while the edge particle flux abruptly increases [38]. These in turn suggest that the degradation and collapse of the ubiquitous edge shear layer are the causes of the abrupt increase in particle transport as $n \to n_G$. This paper calculates the initial edge density for shear layer collapse, and elucidates both the physics of this process and its relation to radiation driven macroscopic phenomena. It extends significantly previous theoretical work on this subject [40]. Here we review the most interesting results.

A striking feature of the Greenwald limit is its strong dependence on current - and almost nothing else. With this in mind, a key outcome of this work is the unification of neoclassical polarization and drift wave - zonal flow dynamics. These have been studied extensively before, but almost always as separate phenomena. Neoclassical polarization and the associated zonal flow screening length were calculated here for banana, plateau and Pfirsch - Schluter regimes, with plateau being the most relevant. The screening length turns out to be $\rho_{sc} = \sqrt{\rho_s^2 + \mathcal{L}\rho_\theta^2}$. Here $\mathcal{L} = 1$ for banana regime, $\mathcal{L} < 1$ for plateau regime and $\mathcal{L} = 0$ for Pfirsch - Schluter regime. The screening lengths in the three regimes compare as $\rho_{sc}^{PS} \ll \rho_{sc}^{plateau} < \rho_{sc}^{banana}$, hence the residual zonal potential strengths compare as

$$\left(\frac{\phi_k(\infty)}{\phi_k(0)}\right)_{Pfirsch-Schluter} \gg \left(\frac{\phi_k(\infty)}{\phi_k(0)}\right)_{plateau} > \left(\frac{\phi_k(\infty)}{\phi_k(0)}\right)_{banana}.$$

Favorable B_θ scaling of the zonal flow screening persists in the plateau regime. A complete dynamical theory - including both modulational response / 'negative viscosity' and incoherent emission / 'zonal noise' effects is presented for the Hasegawa - Wakatani model drift waves with neoclassical zonal response. The modulational growth rate of the zonal flow scales with poloidal field as $\sim B_\theta^2$, while the zonal noise scales as $\sim B_\theta^4$. Using the above, a 'predator-prey' for fluctuation and zonal shear intensity was derived, which includes zonal noise. This extends previous work on similar models [40, 60]. The

model is valid for the adiabatic regime ($\alpha \geq 1$), which is the relevant one, for present day tokamaks.

Using the extended predator-prey system, we identified a criterion for edge shear layer collapse. This condition is for a 'back transition' from a state of turbulence+shear flow to one of strong turbulence without flow, and so defines an effective shear collapse threshold. It is rather puzzling that the Greenwald limit is not cast in terms of a dimensionless ratio. The local zonal shear collapse criterion presented here is, however, and takes the form:

$$\frac{\rho_s}{\sqrt{\rho_{sc}L_n}} < \left[\frac{\eta}{\Omega_i}\frac{\gamma_d}{2k_x^2\rho_s^2\Theta\Omega_i^2}\frac{\hat{\alpha}}{q_\perp^2\rho_s^2}\frac{(1+q_\perp^2\rho_s^2)^3}{q_y^2\rho_s^2}\right]^{1/4}.$$

Here $\rho_s/\sqrt{\rho_{sc}L_n}$ is the fundamental dimensionless ratio, which incorporates the ZF screening length ρ_{sc}. Observe, $\rho_s/\sqrt{\rho_{sc}L_n} = \rho_\star^{1/2}(\rho_s/L_n)^{1/2}$, which increases $\sim (B_\theta/B_T)^{1/2}$, via zonal flow screening physics. We see there is more to life than $\rho_\star$ scaling! Given the relation between fueling and density gradient, which follows from particle balance, we derived a condition for the fueling strength required to sustain the shear layer. This is given in equation(87). The critical integrated dimensionless fueling strength S/nc_s is set by zonal flow damping and scales as $\sim (\rho_{sc}/\rho_s)^3$ -i.e., quite favorably with B_θ. Just as the critical power for the L→H transition gives the threshold for establishing and maintenance of the edge transport barrier (i.e., mean shear layer) [61], $(S/nc_s)_{crit}$ gives the critical fueling strength required to maintain the L-mode edge shear layer against viscous and charge exchange damping.

The principle results of this paper follow directly from the critical value of S/nc_s. For a primarily viscous zonal flow, we obtain a limit on the edge density so as to avoid zonal flow collapse:

$$n < \frac{\rho_s}{\rho_{sc}}\left(\frac{S}{c_s}\right)^{1/3}\left(\frac{n\hat{\alpha}}{q_\perp^2\rho_s^2}\right)^{1/6}\left[\frac{2\Theta\Omega_i^2}{\rho_i^2\nu_{ii}/\rho_s^2 n}\right]^{1/2}\left[\frac{\Omega_i}{\eta}\right]^{1/6}\left[\frac{q_y^2\rho_s^2}{(1+q_\perp^2\rho_s^2)}\right]^{1/6}.$$

For regimes where charge exchange friction is dominant, we find:

$$n < \frac{\rho_s^2}{\rho_{sc}^2}\left(\frac{S}{c_s}\right)^{2/3}\left(\frac{n\hat{\alpha}}{q_\perp^2\rho_s^2}\right)^{1/3}\left[\frac{2k_x^2\rho_s^2\Theta\Omega_i^2}{\gamma_{icx}}\right]\left[\frac{\Omega_i}{\eta}\right]^{1/3}\left[\frac{q_y^2\rho_s^2}{(1+q_\perp^2\rho_s^2)}\right]^{1/3}.$$

These are explicit edge density bounds necessary for shear layer persistence. Note that for viscosity dominant $n_{crit} \sim B_\theta S^{1/3}$, while for charge exchange friction dominant $n_{crit} \sim B_\theta^2 S^{2/3}$. Poloidal field scaling emerges from the zonal flow screening length. These bounds are soft (i.e., transport) limits. While these results are bounds on the (local) edge density, and the Greenwald density is for line averaged density, there are several trends in common. Given that the bounds are on the local density and $\rho_s/\sqrt{\rho_{sc}L_n}$ is identified as the relevant dimensionless ratio, we (boldly) suggest that these results encapsulate the key transport physics underpinning the Greenwald limit.

Of course, one could in principle support the edge shear layer by increasing S/nc_s. This, however, leads to enhanced cooling and a concomitant increase in edge radiation to the point where MARFE's and /or radiation driven magnetic islands and disruption occurs. The feedback loop governing this evolution is identified, discussed, and shown in figure(7). The fundamental point here is that MARFEs, magnetic islands etc. are secondary to transport physics.

These results have implications for devices other than tokamaks. This follows from the fact that the model developed here links density limit to the edge shear layer, which is present in all known devices. The edge shear layer, in turn, is controlled (in part) by the zonal flow screening response. In stellarators, the principal correction to classical screening is due to helically trapped particles. This has no obvious length scale [62] other than ρ_i, so the zonal flow screening is classical. Thus the "effective inertia" for zonal flows in stellerators is lower than that for tokamks. Hence, for equal excitation and damping, we expect zonal flow shears in stellerators to be stronger than those in tokamaks. This feature likely explains why attempts to link stellarator density limits to

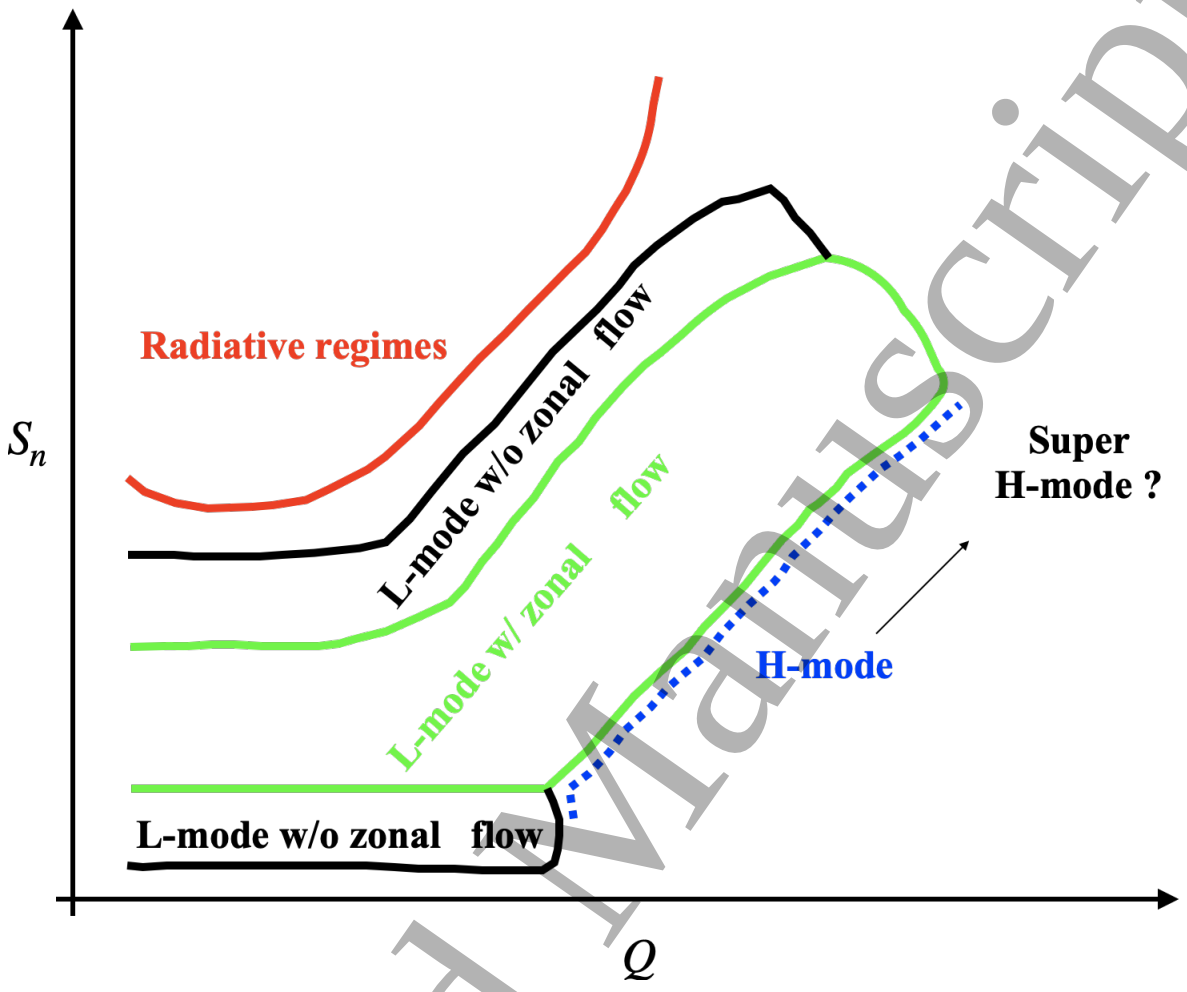

Figure 8. A sketch of the 'phase diagram' characterizing the states of the tokamak edge in S_n - Q space.

magnetic geometry have failed, and why stellarator density limits are higher than those for tokamaks.

Towards the 'big picture', the analysis of this paper suggests a 'phase diagram' approach to the characterization of the states of the tokamak edge. The phase diagram is drawn in the space of edge fueling S and core heat flux (input power) Q, which are the two fundamental control parameters. All of the L→H transition, L-mode with and without shear layer and the density limit regime can be unified in this way. A schematic phase diagram is sketched in figure(8).

At this point, it is appropriate to suggest some experiments relevant to shear

layer collapse. In addition to direct tests of the n_{crit} and $S_{n,crit}$, predictions in this paper, one might also study the scale of shear layer collapse, and its correlation with ρ_{sc}. Perturbative experiments would be very interesting. One of these could repeat the pellet/SMBI experiment of Greenwald [27], along with relevant fluctuation measurements. The aim is to relate the density relaxation time to predictions based on transport dynamics. Another is to explore RMP effects on shear layer collapse. For example, is the critical edge density with RMP lower than without? Is this because zonal shears are already weekend by the RMP [63]? Finally, one could explore if edge biasing can sustain an $\overline{n} > n_G$ (or $n_{edge} > n_{crit}$) by driving the edge shear layer, externally. This technique has been shown to allow achieving H - mode - like states with good particle confinement, at modest power [64–66]. Could biasing allow one to beat the Greenwald limit? And is the shear layer collapse transport bifurcation hysteretic or not? Work on all of these questions could help illuminate the transport physics of the density limit.

There are several directions for future work on shear layer collapse. One is a more detailed and quantitative rendering of the phase diagram, discussed above. Of course, one can pursue more detailed models, with more effects etc. Questions concerning the interplay of B_θ scaling via ρ_{sc} with B_θ scaling via $k_\| \sim 1/qR$ (i.e., from Landau damping!?) arise naturally. More interestingly, this analysis is not relevant to the critical question of the H - mode density limit (HDL) [29, 30], where an explanation of mean $E \times B$ shear layer collapse and the subsequent back transition is needed. This is a key question for ITER and other future devices. En route to this, the fascinating phenomenon whereby the plasma seems to always back-transition from H to L prior to hitting the Greenwald limit remains to be understood. We speculate that this phenomenon may be related to the structure of the (Q, S) phase diagram, which is fundamental to both the density limit and the L→H transition. These questions, and

others, will be pursued in future publications.

Finally, we note that Rice *et al* [13] recently showed that much of the Ohmic phenomenology (i.e., LOC-SOC phenomenology, rotation reversal etc.) may be unified by the scaling relation $n_{crit}qR = B_T$ which is easily seen to be equivalent to $n/n_G = const$, where n_G is Greenwald density and the constant is $\mathcal{O}(1/2)$. The familiar Greenwald limit phenomenology (as opposed to the Ohmic confinement phenomenology) -i.e., radiative cooling, Marfes, disruption etc., - set in for $n/n_G \sim \mathcal{O}(1)$. Thus, we have a dilemma! Why the similarity to the Greenwald scalings, but for phenomena which occur at lower density? We speculate here that the resolution may be the onset of edge shear layer decay and collapse, accompanied by an increase in particle transport. These occur for $n/n_G < 1$ (but not $n/n_G \ll 1$), and often are a precursor to the more violent phenomena associated with the density limit. Indeed, in Ref [38], shear layer decay is noticeable for $n/n_G \sim 0.6$. Edge shear layer decay may impact the degree of density profile peaking. This in turn will impact global confinement. Furthermore, recall observation that $n_{crit}qR \sim B_T$ appears to be related to the minimum in the power threshold P_{th} for L→H transition [67, 68]. We speculate that this may be due to the onset of pre-transition shear layer decay for $n/n_G < 1$. This in turn weakens the 'seed' shear which initiates the L→H transition, and thus necessitates an increase in the power required for the transition. These observations and speculations suggest a link between the strength of the Ohmic / L-mode edge shear layer, and the global state of confinement. In retrospect, this should not be so surprising. We plan to investigate these questions in depth in future work.

Acknowledgments

We thank Martin Greenwald and John Rice for many fascinating discussions concerning density limit physics and Ohmic phenomenology and Taik-Soo Hahm for discussions on zonal flow screening response. We also thank Ting Long, Rui Ke, Rima Hajjar, Mikhail Malkov, George Tynan, Hongjuan Sun, Jim Myra, Sergei Krasheninnikov, Ozgur Gurcan, Pascale Hennequin and Lu Wang for interesting comments and discussions. Discussions with participants in the Festival de Theory 2017 and 2019 are acknowledged. This research was supported by U.S. DOE under Award No. $DE-FG02-04ER54738$.

[1] Wagner F 2018 *The European Physical Journal H* **43** 523–549 URL https://doi.org/10.1140/epjh/e2016-70064-9

[2] Wagner F, Becker G, Behringer K, Campbell D, Eberhagen A, Engelhardt W, Fussmann G, Gehre O, Gernhardt J, Gierke G v, Haas G, Huang M, Karger F, Keilhacker M, Klüber O, Kornherr M, Lackner K, Lisitano G, Lister G G, Mayer H M, Meisel D, Müller E R, Murmann H, Niedermeyer H, Poschenrieder W, Rapp H, Röhr H, Schneider F, Siller G, Speth E, Stäbler A, Steuer K H, Venus G, Vollmer O and Yü Z 1982 *Phys. Rev. Lett.* **49**(19) 1408–1412 URL https://link.aps.org/doi/10.1103/PhysRevLett.49.1408

[3] Wagner F 2007 *Plasma Physics and Controlled Fusion* **49** B1–B33 URL https://doi.org/10.1088/0741-3335/49/12b/s01

[4] Kaye S, Bell M, Bol K, Boyd D, Brau K, Buchenauer D, Budny R, Cavallo A, Couture P, Crowley T, Darrow D, Eubank H, Fonck R, Goldston R, Grek B, Jaehnig K, Johnson D, Kaita R, Kugel H, Leblanc B, Manickam J, Manos D, Mansfield D, Mazzucato E, McCann R, McCune D, McGuire K, Mueller D, Murdock A, Okabayashi M, Okano K, Owens D, Post D, Reusch M, Schmidt G, Sesnic S, Slusher R, Suckewer S, Surko C, Takahashi H, Tenney F, Towner H and Valley J 1984 *Journal of Nuclear Materials* **121** 115–125 ISSN 0022-3115 URL https://www.sciencedirect.com/science/article/pii/0022311584901119

[5] Erckmann V, Wagner F, Baldzuhn J, Brakel R, Burhenn R, Gasparino U, Grigull P, Hartfuss H J, Hofmann J V, Jaenicke R, Niedermeyer H, Ohlendorf W, Rudyj A, Weller A, Bogdanov S D, Bomba B, Borschegovsky A A, Cattanei G, Dodhy A, Dorst D, Elsner A, Endler M, Geist T, Giannone L, Hacker H, Heinrich O, Herre G, Hildebrandt D, Hiznyak V I,

Il'in V I, Kasparek W, Karger F, Kick M, Kubo S, Kuftin A N, Kurbatov V I, Lazaros A, Malygin S A, Malygin V I, McCormick K, Müller G A, Orlov V B, Pech P, Roi I N, Sardei F, Sattler S, Schneider F, Schneider U, Schüller P G, Siller G, Stroth U, Tutter M, Unger E, Wolff H, Würsching E and Zöpfel S 1993 *Phys. Rev. Lett.* **70**(14) 2086–2089 URL https://link.aps.org/doi/10.1103/PhysRevLett.70.2086

[6] Taylor R J, Brown M L, Fried B D, Grote H, Liberati J R, Morales G J, Pribyl P, Darrow D and Ono M 1989 *Phys. Rev. Lett.* **63**(21) 2365–2368 URL https://link.aps.org/doi/10.1103/PhysRevLett.63.2365

[7] Conway G D, Angioni C, Ryter F, Sauter P and Vicente J (ASDEX Upgrade Team) 2011 *Phys. Rev. Lett.* **106**(6) 065001 URL https://link.aps.org/doi/10.1103/PhysRevLett.106.065001

[8] Schmitz L, Zeng L, Rhodes T L, Hillesheim J C, Doyle E J, Groebner R J, Peebles W A, Burrell K H and Wang G 2012 *Phys. Rev. Lett.* **108**(15) 155002 URL https://link.aps.org/doi/10.1103/PhysRevLett.108.155002

[9] Strachan J D, Bitter M, Ramsey A T, Zarnstorff M C, Arunasalam V, Bell M G, Bretz N L, Budny R, Bush C E, Davis S L, Dylla H F, Efthimion P C, Fonck R J, Fredrickson E, Furth H P, Goldston R J, Grisham L R, Grek B, Hawryluk R J, Heidbrink W W, Hendel H W, Hill K W, Hsuan H, Jaehnig K P, Jassby D L, Jobes F, Johnson D W, Johnson L C, Kaita R, Kampershroer J, Knize R J, Kozub T, LeBlanc B, Levinton F, La Marche P H, Manos D M, Mansfield D K, McGuire K, McNeill D H, Meade D M, Medley S S, Morris W, Mueller D, Nieschmidt E B, Owens D K, Park H, Schivell J, Schilling G, Schmidt G L, Scott S D, Sesnic S, Sinnis J C, Stauffer F J, Stratton B C, Tait G D, Taylor G, Towner H H, Ulrickson M, von Goeler S, Wieland R, Williams M D, Wong K L, Yoshikawa S, Young K M and Zweben S J 1987 *Phys. Rev. Lett.* **58**(10) 1004–1007 URL https://link.aps.org/doi/10.1103/PhysRevLett.58.1004

[10] Söldner F X, Müller E R, Wagner F, Bosch H S, Eberhagen A, Fahrbach H U, Fussmann G, Gehre O, Gentle K, Gernhardt J, Gruber O, Herrmann W, Janeschitz G, Kornherr M, Krieger K, Mayer H M, McCormick K, Murmann H D, Neuhauser J, Nolte R, Poschenrieder W, Röhr H, Steuer K H, Stroth U, Tsois N and Verbeek H 1988 *Phys. Rev. Lett.* **61**(9) 1105–1108 URL https://link.aps.org/doi/10.1103/PhysRevLett.61.1105

[11] Whyte D, Hubbard A, Hughes J, Lipschultz B, Rice J, Marmar E, Greenwald M, Cziegler I, Dominguez A, Golfinopoulos T, Howard N, Lin L, McDermott R, Porkolab M, Reinke M, Terry J, Tsujii N, Wolfe S, Wukitch S and and Y L 2010 *Nuclear Fusion* **50** 105005 URL

https://doi.org/10.1088/0029-5515/50/10/105005

[12] Parker R, Greenwald M, Luckhardt S, Marmar E, Porkolab M and Wolfe S 1985 *Nuclear Fusion* **25** 1127–1136 URL https://doi.org/10.1088/0029-5515/25/9/023

[13] Rice J, Citrin J, Cao N, Diamond P, Greenwald M and Grierson B 2020 *Nuclear Fusion* **60** 105001 URL https://doi.org/10.1088/1741-4326/abac4b

[14] Messiaen A, Ongena J, Samm U, Unterberg B, Vandenplas P, Oost G V, Wassenhove G V, Winter J, Boucher D, Dumortier P, Durodie F, Esser H, Euringer H, Giesen B, Hintz E, Lochter M, Tokar M, Wolf G, Fuchs G, Hillis D, Hoenen F, Huttemann P, Koch R, Konen L, Koslowski H, Kramer-Flecken A, Pettiaux D, Pospieszczyk A, Schweer B, Soltwisch H, Telesca G, Uhlemann R, van Nieuwenhove R, Vervier M, Waidmann G and Weynants R 1994 *Nuclear Fusion* **34** 825–836 URL https://doi.org/10.1088/0029-5515/34/6/i06

[15] Greenwald M, Gwinn D, Milora S, Parker J, Parker R, Wolfe S, Besen M, Camacho F, Fairfax S, Fiore C, Foord M, Gandy R, Gomez C, Granetz R, LaBombard B, Lipschultz B, Lloyd B, Marmar E, McCool S, Pappas D, Petrasso R, Pribyl P, Rice J, Schuresko D, Takase Y, Terry J and Watterson R 1984 *Phys. Rev. Lett.* **53**(4) 352–355 URL https://link.aps.org/doi/10.1103/PhysRevLett.53.352

[16] Weynants R, Messiaen A, Ongena J, Unterberg B, Bonheure G, Dumortier P, Jaspers R, Koch R, Koslowski H, KrÃ€mer-Flecken A, Mank G, Rapp J, Tokar' M, Wassenhove G V, Biel W, Brix M, Durodié F, Esser G, Finken K, Fuchs G, Giesen B, Hobirk J, HÃŒttemann P, Lehnen M, Lyssoivan A, Mertens P, Pospieszczyk A, Samm U, Sauer M, Schweer B, Uhlemann R, Oost G V, Vandenplas P, Vervier M, Philipps V, Waidmann G and Wolf G 1999 *Nuclear Fusion* **39** 1637–1648 URL https://doi.org/10.1088/0029-5515/39/11y/303

[17] Jackson G L, Winter J, Taylor T S, Burrell K H, DeBoo J C, Greenfield C M, Groebner R J, Hodapp T, Holtrop K, Lazarus E A, Lao L L, Lippmann S I, Osborne T H, Petrie T W, Phillips J, James R, Schissel D P, Strait E J, Turnbull A D, West W P and Team D D 1991 *Phys. Rev. Lett.* **67**(22) 3098–3101 URL https://link.aps.org/doi/10.1103/PhysRevLett.67.3098

[18] Gruber O, Kallenbach A, Kaufmann M, Lackner K, Mertens V, Neuhauser J, Ryter F, Zohm H, Bessenrodt-Weberpals M, Büchl K, Fiedler S, Field A, Fuchs C, Garcia-Rosales C, Haas G, Herrmann A, Herrmann W, Hirsch S, Köppendörfer W, Lang P, Lieder G, Mast K F, Pitcher C S, Schittenhelm M, Stober J, Suttrop W, Troppmann M, Weinlich M, Albrecht M, Alexander M, Asmussen K, Ballico M, Behler K, Behringer K, Bosch H S, Brambilla M, Carlson A, Coster D,

Cupido L, DeBlank H J, De Pena Hempel S, Deschka S, Dorn C, Drube R, Dux R, Eberhagen A, Engelhardt W, Fahrbach H U, Feist H U, Fieg D, Fußmann G, Gehre O, Gernhardt J, Ignacz P, Jüttner B, Junker W, Kass T, Kiemer K, Kollotzek H, Kornherr M, Krieger K, Kurzan B, Lang R, Laux M, Manso M E, Maraschek M, Mayer H M, McCarthy P, Meisel D, Merkel R, Murmann H, Napiontek B, Naujoks D, Neu G, Neu R, Noterdaeme J M, Pautasso G, Poschenrieder W, Raupp G, Richter H, Richter T, Röhr H, Roth J, Salmon N, Salzmann H, Sandmann W, Schilling H B, Schneider H, Schneider R, Schneider W, Schönmann K, Schramm G, Schumacher U, Schweinzer J, Seidel U, Serra F, Silva A, Sokoll M, Speth E, Stäbler A, Steuer K H, Streibl B, Treutterer W, Ulrich M, Varela P, Vernickel H, Vollmer O, Wedler H, Wenzel U, Wesner F, Wunderlich R, Zasche D and Zehrfeld H P 1995 *Phys. Rev. Lett.* **74**(21) 4217–4220 URL https://link.aps.org/doi/10.1103/PhysRevLett.74.4217

[19] Burrell K H, Austin M E, Brennan D P, DeBoo J C, Doyle E J, Fenzi C, Fuchs C, Gohil P, Greenfield C M, Groebner R J, Lao L L, Luce T C, Makowski M A, McKee G R, Moyer R A, Petty C C, Porkolab M, Rettig C L, Rhodes T L, Rost J C, Stallard B W, Strait E J, Synakowski E J, Wade M R, Watkins J G and West W P 2001 *Physics of Plasmas* **8** 2153–2162 (*Preprint* https://doi.org/10.1063/1.1355981) URL https://doi.org/10.1063/1.1355981

[20] Burrell K H, Barada K, Chen X, Garofalo A M, Groebner R J, Muscatello C M, Osborne T H, Petty C C, Rhodes T L, Snyder P B, Solomon W M, Yan Z and Zeng L 2016 *Physics of Plasmas* **23** 056103 (*Preprint* https://doi.org/10.1063/1.4943521) URL https://doi.org/10.1063/1.4943521

[21] Connor J, Fukuda T, Garbet X, Gormezano C, Mukhovatov V, Wakatani M, the ITB Database Group, the ITPA Topical Group on Transport and Physics I B 2004 *Nuclear Fusion* **44** R1–R49 URL https://doi.org/10.1088/0029-5515/44/4/r01

[22] Koide Y, Kikuchi M, Mori M, Tsuji S, Ishida S, Asakura N, Kamada Y, Nishitani T, Kawano Y, Hatae T, Fujita T, Fukuda T, Sakasai A, Kondoh T, Yoshino R and Neyatani Y 1994 *Phys. Rev. Lett.* **72**(23) 3662–3665 URL https://link.aps.org/doi/10.1103/PhysRevLett.72.3662

[23] Levinton F M, Zarnstorff M C, Batha S H, Bell M, Bell R E, Budny R V, Bush C, Chang Z, Fredrickson E, Janos A, Manickam J, Ramsey A, Sabbagh S A, Schmidt G L, Synakowski E J and Taylor G 1995 *Phys. Rev. Lett.* **75**(24) 4417–4420 URL https://link.aps.org/doi/10.1103/PhysRevLett.75.4417

[24] Strait E J, Lao L L, Mauel M E, Rice B W, Taylor T S, Burrell K H, Chu M S, Lazarus E A,

Osborne T H, Thompson S J and Turnbull A D 1995 *Phys. Rev. Lett.* **75**(24) 4421–4424 URL https://link.aps.org/doi/10.1103/PhysRevLett.75.4421

[25] Austin M E, Marinoni A, Walker M L, Brookman M W, deGrassie J S, Hyatt A W, McKee G R, Petty C C, Rhodes T L, Smith S P, Sung C, Thome K E and Turnbull A D 2019 *Phys. Rev. Lett.* **122**(11) 115001 URL https://link.aps.org/doi/10.1103/PhysRevLett.122.115001

[26] Troyon F, Roy A, Cooper W A, Yasseen F and Turnbull A 1988 *Plasma Physics and Controlled Fusion* **30** 1597–1609 URL https://doi.org/10.1088/0741-3335/30/11/019

[27] Greenwald M, Terry J, Wolfe S, Ejima S, Bell M, Kaye S and Neilson G 1988 *Nuclear Fusion* **28** 2199–2207 URL https://doi.org/10.1088/0029-5515/28/12/009

[28] Hender T, Wesley J, Bialek J, Bondeson A, Boozer A, Buttery R, Garofalo A, Goodman T, Granetz R, Gribov Y, Gruber O, Gryaznevich M, Giruzzi G, GÃŒnter S, Hayashi N, Helander P, Hegna C, Howell D, Humphreys D, Huysmans G, Hyatt A, Isayama A, Jardin S, Kawano Y, Kellman A, Kessel C, Koslowski H, Haye R L, Lazzaro E, Liu Y, Lukash V, Manickam J, Medvedev S, Mertens V, Mirnov S, Nakamura Y, Navratil G, Okabayashi M, Ozeki T, Paccagnella R, Pautasso G, Porcelli F, Pustovitov V, Riccardo V, Sato M, Sauter O, Schaffer M, Shimada M, Sonato P, Strait E, Sugihara M, Takechi M, Turnbull A, Westerhof E, Whyte D, Yoshino R, Zohm H, the ITPA MHD D and Group M 2007 *Nuclear Fusion* **47** S128–S202 URL https://doi.org/10.1088/0029-5515/47/6/s03

[29] Bernert M, Eich T, Kallenbach A, Carralero D, Huber A, Lang P T, Potzel S, Reimold F, Schweinzer J, Viezzer E and Zohm H 2014 *Plasma Physics and Controlled Fusion* **57** 014038 URL https://doi.org/10.1088/0741-3335/57/1/014038

[30] Huber A, Bernert M, Brezinsek S, Chankin A, Sergienko G, Huber V, Wiesen S, Abreu P, Beurskens M, Boboc A, Brix M, Calabro G, Carralero D, Delabie E, Eich T, Esser H, Groth M, Guillemaut C, Jachmich S, JÃ€rvinen A, Joffrin E, Kallenbach A, Kruezi U, Lang P, Linsmeier C, Lowry C, Maggi C, Matthews G, Meigs A, Mertens P, Reimold F, Schweinzer J, Sips G, Stamp M, Viezzer E, Wischmeier M and Zohm H 2017 *Nuclear Materials and Energy* **12** 100 – 110 ISSN 2352-1791 proceedings of the 22nd International Conference on Plasma Surface Interactions 2016, 22nd PSI URL http://www.sciencedirect.com/science/article/pii/S2352179116300588

[31] Goldston R 2015 *Journal of Nuclear Materials* **463** 397–400 ISSN 0022-3115 pLASMA-SURFACE INTERACTIONS 21 URL https://www.sciencedirect.com/science/article/pii/S0022311514007648

[32] Eich T, Goldston R, Kallenbach A, Sieglin B, Sun H and and 2018 *Nuclear Fusion* **58** 034001 URL https://doi.org/10.1088/1741-4326/aaa340

[33] Sun H J, Goldston R J, Huber A, Xu X Q, Flanagan J, McDonald D C, de la Luna E, Maslov M, Harrison J, Militello F, Fessey J, Cramp S and Contributors J 2021 *Nuclear Fusion* (**under review**)

[34] Greenwald M 2002 *Plasma Physics and Controlled Fusion* **44** R27–R53 URL https://doi.org/10.1088/0741-3335/44/8/201

[35] Drake J F 1987 *The Physics of Fluids* **30** 2429–2433 (*Preprint* https://aip.scitation.org/doi/pdf/10.1063/1.866133) URL https://aip.scitation.org/doi/abs/10.1063/1.866133

[36] Gates D A and Delgado-Aparicio L 2012 *Phys. Rev. Lett.* **108**(16) 165004 URL https://link.aps.org/doi/10.1103/PhysRevLett.108.165004

[37] Xu Y, Carralero D, Hidalgo C, Jachmich S, Manz P, Martines E, van Milligen B, Pedrosa M, Ramisch M, Shesterikov I, Silva C, Spolaore M, Stroth U and Vianello N 2011 *Nuclear Fusion* **51** 063020 URL https://doi.org/10.1088/0029-5515/51/6/063020

[38] Hong R, Tynan G, Diamond P, Nie L, Guo D, Long T, Ke R, Wu Y, Yuan B and and M X 2017 *Nuclear Fusion* **58** 016041 URL https://doi.org/10.1088/1741-4326/aa9626

[39] Schmid B, Manz P, Ramisch M and Stroth U 2017 *Phys. Rev. Lett.* **118**(5) 055001 URL https://link.aps.org/doi/10.1103/PhysRevLett.118.055001

[40] Hajjar R J, Diamond P H and Malkov M A 2018 *Physics of Plasmas* **25** 062306 (*Preprint* https://doi.org/10.1063/1.5030345) URL https://doi.org/10.1063/1.5030345

[41] Vallis G K and Maltrud M E 1993 *Journal of Physical Oceanography* **23** 1346–1362 ISSN 0022-3670 (*Preprint* https://journals.ametsoc.org/jpo/article-pdf/23/7/1346/4423462/1520-0485(1993)023_1346_gomfaj_2_0_co_2.pdf) URL https://doi.org/10.1175/1520-0485(1993)023<1346:GOMFAJ>2.0.CO;2

[42] Camargo S J, Biskamp D and Scott B D 1995 *Phys. Plasmas* **2** 48–62

[43] Xu X Q, Nevins W M, Rognlien T D, Bulmer R H, Greenwald M, Mahdavi A, Pearlstein L D and Snyder P 2003 *Physics of Plasmas* **10** 1773–1781 (*Preprint* https://doi.org/10.1063/1.1566032) URL https://doi.org/10.1063/1.1566032

[44] Numata R, Ball R and Dewar R L 2007 *Physics of Plasmas* **14** 102312 (*Preprint* https://doi.org/10.1063/1.2796106) URL https://doi.org/10.1063/1.2796106

[45] Pushkarev A V, Bos W J T and Nazarenko S V 2013 *Physics of Plasmas* **20** 042304 (*Preprint*

https://doi.org/10.1063/1.4802187) URL https://doi.org/10.1063/1.4802187

[46] Ghantous K and Gürcan O D 2015 *Phys. Rev. E* **92**(3) 033107 URL https://link.aps.org/doi/10.1103/PhysRevE.92.033107

[47] Long T, Diamond P, Xu M, Ke R, Nie L, Li B, Wang Z, Xu J and and X D 2019 *Nuclear Fusion* **59** 106010 URL https://doi.org/10.1088%2F1741-4326%2Fab33cf

[48] Singh R and Diamond P H 2021 *Plasma Physics and Controlled Fusion* **63** 035015 URL https://doi.org/10.1088/1361-6587/abd618

[49] Rosenbluth M N and Hinton F L 1998 *Phys. Rev. Lett.* **80** 724–727

[50] Hinton F L and Rosenbluth M N 1999 *Plasma Physics and Controlled Fusion* **41** A653 URL http://stacks.iop.org/0741-3335/41/i=3A/a=059

[51] Xiao Y, Catto P J and Molvig K 2007 *Physics of Plasmas* **14** 032302 (*Preprint* https://doi.org/10.1063/1.2536297) URL https://doi.org/10.1063/1.2536297

[52] Hasegawa A and Wakatani M 1983 *Phys. Rev. Lett.* **50**(9) 682–686 URL https://link.aps.org/doi/10.1103/PhysRevLett.50.682

[53] Wakatani M and Hasegawa A 1984 *The Physics of Fluids* **27** 611–618 (*Preprint* https://aip.scitation.org/doi/pdf/10.1063/1.864660) URL https://aip.scitation.org/doi/abs/10.1063/1.864660

[54] Hasegawa A and Mima K 1978 *Phys. Fluids* **21** 87–92

[55] Diamond P H, S-I Itoh, Itoh K and Hahm T S 2005 *Plasma. Phys. Cont* **47** R35–R161

[56] Rebut P H and Hugon M 1985 *Plasma Physics and Controlled Nuclear Fusion Research, Tenth Conference Proceedings, London, 12-19 September 1984* **2** 197 URL http://www-naweb.iaea.org/napc/physics/FEC/STIPUB670_VOL2.pdf

[57] Gates D A, Brennan D P, Delgado-Aparicio L, Teng Q and White R B 2016 *Physics of Plasmas* **23** 056113 (*Preprint* https://doi.org/10.1063/1.4948624) URL https://doi.org/10.1063/1.4948624

[58] Charlton L A, Carreras B A, Lynch V E, Sidikman K L and Diamond P H 1994 *Physics of Plasmas* **1** 2700–2710 (*Preprint* https://doi.org/10.1063/1.870597) URL https://doi.org/10.1063/1.870597

[59] Lin Z, Hahm T S, Lee W W, Tang W M and Diamond P H 1999 *Phys. Rev. Lett.* **83** 3645–3648

[60] Diamond P H, Liang Y M, Carreras B A and Terry P W 1994 *Phys. Rev. Lett.* **72** 2565–2568

[61] Hinton F L 1991 *Physics of Fluids B: Plasma Physics* **3** 696–704 (*Preprint* https://doi.org/10.

1063/1.859866) URL https://doi.org/10.1063/1.859866

[62] Sugama H and Watanabe T H 2005 *Phys. Rev. Lett.* **94**(11) 115001 URL https://link.aps.org/doi/10.1103/PhysRevLett.94.115001

[63] Kriete D M, McKee G R, Schmitz L, Smith D R, Yan Z, Morton L A and Fonck R J 2020 *Physics of Plasmas* **27** 062507 (*Preprint* https://doi.org/10.1063/1.5145207) URL https://doi.org/10.1063/1.5145207

[64] Hidalgo C, Pedrosa M A, Dreval N, McCarthy K J, Eliseev L, Ochando M A, Estrada T, Pastor I, Ascasíbar E, Calderón E, Cappa A, Chmyga A A, Fernández A, Gonçalves B, Herranz J, Jiménez J A, Khrebtov S M, Komarov A D, Kozachok A S, Krupnik L, López-Fraguas A, López-Sánchez A, Melnikov A V, Medina F, van Milligen B, Silva C, Tabarés F and Tafalla D 2003 *Plasma Physics and Controlled Fusion* **46** 287–297 URL https://doi.org/10.1088/0741-3335/46/1/018

[65] Oost G V, mek J A, Antoni V, Balan P, Boedo J A, Devynck P, uran I, Eliseev L, Gunn J P, Hron M, Ionita C, Jachmich S, Kirnev G S, Martines E, Melnikov A, Schrittwieser R, Silva C, ckel J S, Tendler M, Varandas C, Schoor M V, Vershkov V and Weynants R R 2003 *Plasma Physics and Controlled Fusion* **45** 621–643 URL https://doi.org/10.1088/0741-3335/45/5/308

[66] Kitajima S, Takahashi H, Tanaka Y, Utoh H, Sasao M, Takayama M, Nishimura K, Inagaki S and Yokoyama M 2006 *Nuclear Fusion* **46** 200–206 URL https://doi.org/10.1088/0029-5515/46/2/002

[67] Ma Y, Hughes J, Hubbard A, LaBombard B, Churchill R, Golfinopolous T, Tsujii N and Marmar E 2012 *Nuclear Fusion* **52** 023010 URL https://doi.org/10.1088/0029-5515/52/2/023010

[68] Hughes J, Loarte A, Reinke M, Terry J, Brunner D, Greenwald M, Hubbard A, LaBombard B, Lipschultz B, Ma Y, Wolfe S and Wukitch S 2011 *Nuclear Fusion* **51** 083007 URL https://doi.org/10.1088/0029-5515/51/8/083007